EXPERIMENTAL STUDY OF UNIFORM AND CORRUGATED ROD AS SURFACE WAVEGUIDE AND AS RADIATOR *

By K. N. SHANKARA AND S. K. CHATTERJEE
(*Indian Institute of Science, Bangalore-12*)

[Received : April 20, 1972]

1. ABSTRACT

Experimental results are presented on the radial and axial field distributions and hence radial decay coefficient, guide wavelength and also radiation patterns and gain as functions of spacing, depth of grooves, diameter and length of a corrugated rod and also as functions of diameter and length of a uniform rod, both the rods being excited in E_0*-mode. The characteristics such as scattering parameters and hence launching efficiency, etc. of mode transducer used for exciting the uniform and corrugated rods are also determined.*

2. INTRODUCTION

The surface wave characteristics and radiation characteristics of uniform and corrugated dielectric rods have been studied theoretically by the authors and the results are reported elsewhere[1,2]. The object of this paper is to verify the theoretical results experimentally. The experiment is concerned with the measurement of field distribution, radiation pattern and gain of a large number of rods of the above two types (See Appendix A.1). (See Fig. 1 for corrugated rods).

3. MEASUREMENT OF FIELD DISTRIBUTION

The launching unit, its associated assembly and the arrangement for measuring field distribution are shown in Figures 2–4. The field distributions in the axial and radial directions were measured with the aid of a dipole and a monopole probe respectively.

4. GUIDE WAVELENGTH

The guide wavelength λg was determined from the field distributions in the axial direction. The theoretical and measured values of λg are compared in Table 1.

* The project is supported by PL-480, Contract No. E-262-69(N), dated June 15, 1969.

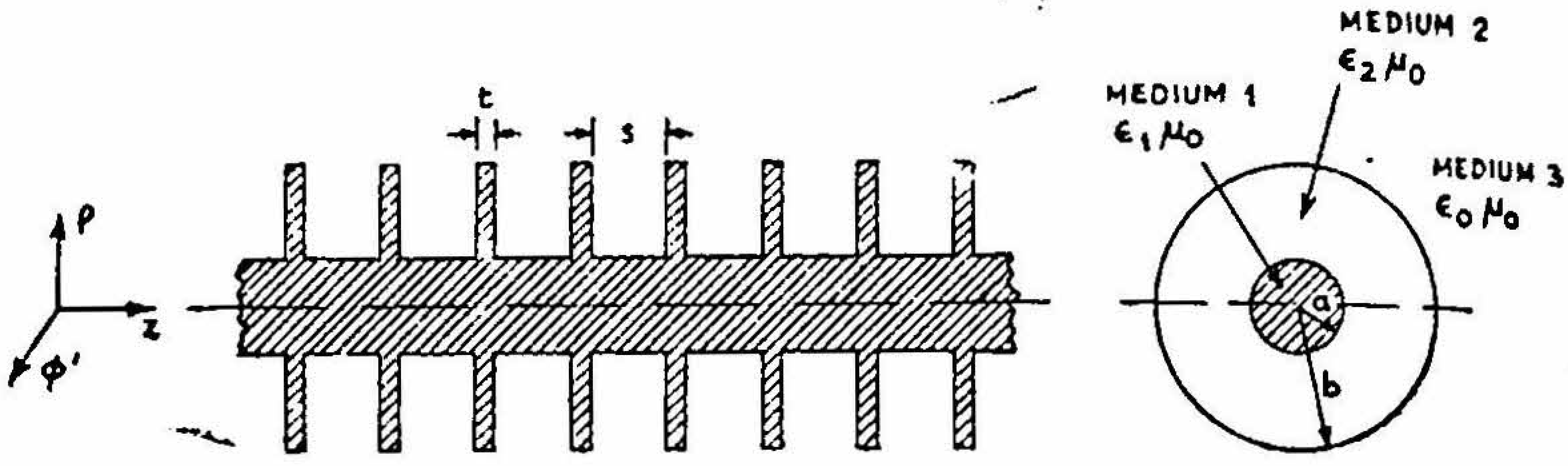

FIG. 1

a = Radius of the inner rod.
b = Radius of disc.
t = Thickness of disc.
s = Spacing between discs.
ϵ_1 = Permittivity of medium 1.
ϵ_2 = Permittivity of medium 2.
ϵ_0 = Permittivity of free space (mediun 3)
μ = Permeability of free space.
Medium 1 ; $\rho \leqslant a$
Medium 2 : $a \leqslant \rho \leqslant b$
Medium 3 : $\rho \geqslant b$

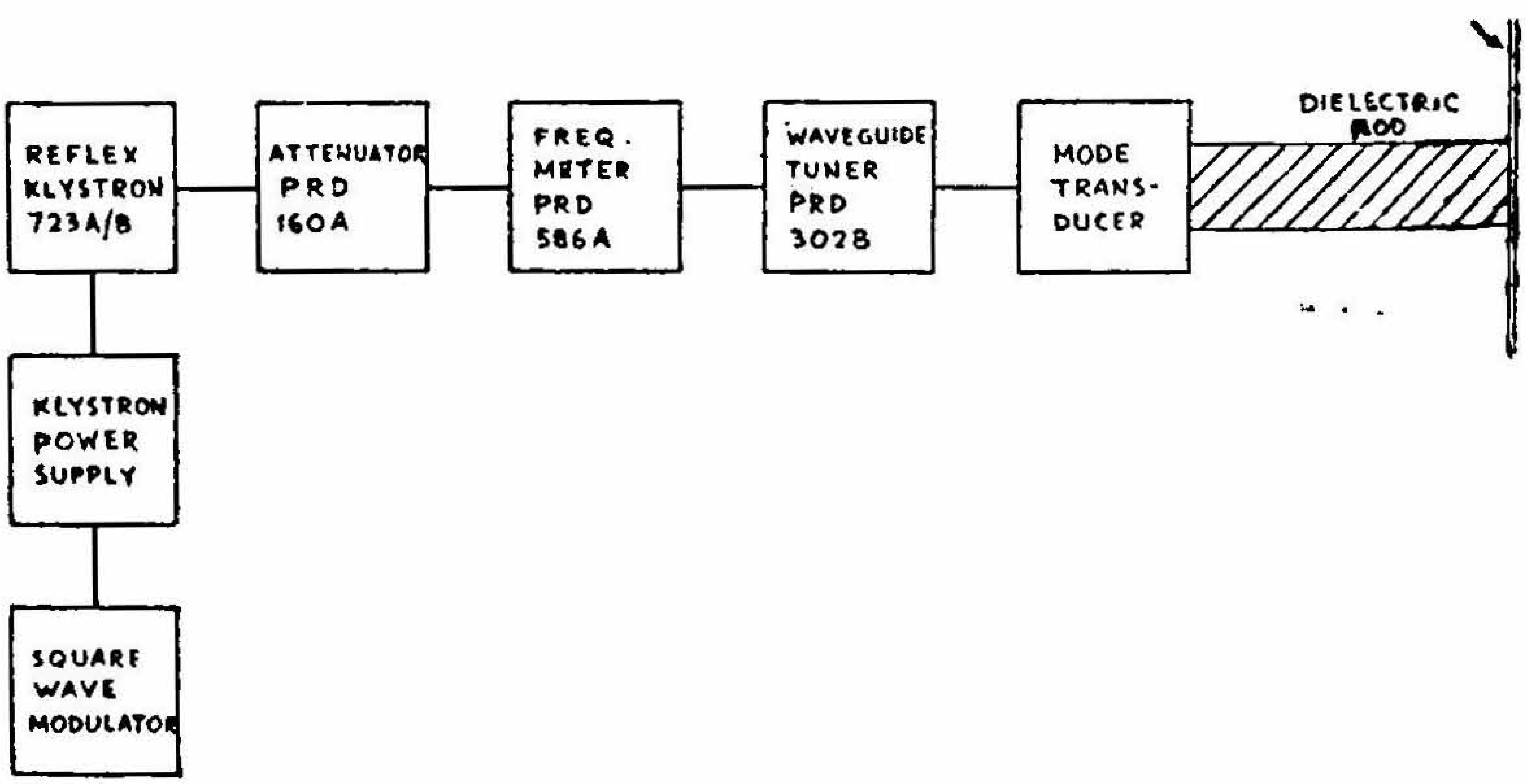

FIG. 2

Block diagram of surface wave launching unit.

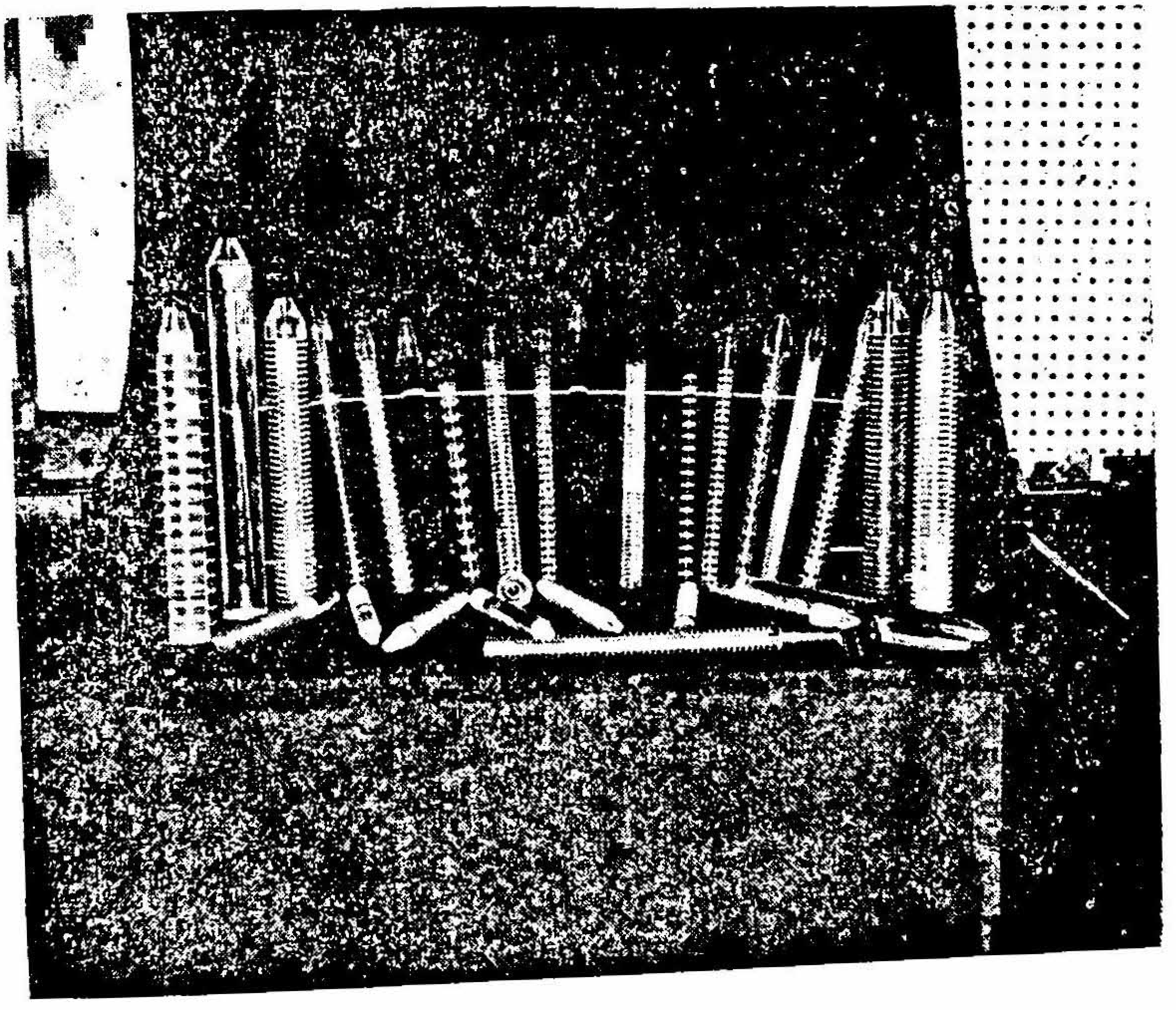

FIG. 3
Corrugated dielectric rod.

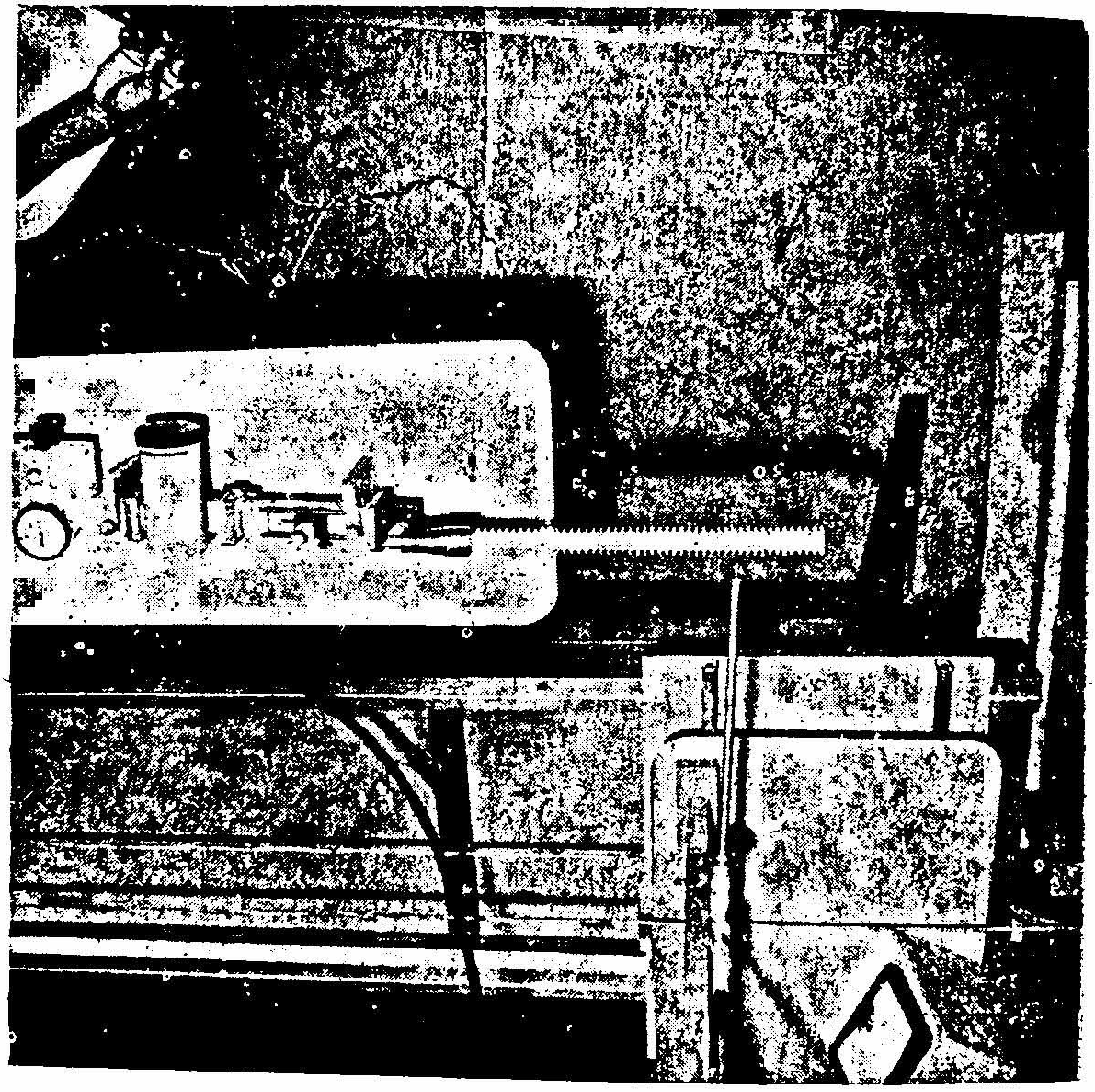

FIG. 4
Measurement of guide wavelength

TABLE 1

Measured and calculated values of λg

Structure Number	Measured λg (cm)	Theoretical λg (cm)	Structure Number	Measured λg (cm)	Theoretical λg (cm)
1 u	2.9	2.902	6 C	2.78	2.7836
7 u	2.82	2.82	7 C	2.70	2.7016
8 u	2.70	2.656	8 C	2.56	2.568
9 u	2.38	2.369	9 C	3.05	3.13
10 u	2.30	2.254	10 C	3.20	3.1084
11 u	2.20	2.1835	11 C	3.05	3.016
12 u	2.16	2.133	12 C	3.05	3 0399
1 C	3.06	2.975	13 C	3.10	2.0165
2 C	3.0	3.07	14 C	3.07	3.08
3 C	3.12	3.088	15 C	2.75	2.788
4 C	3.05	3.0998	16 C	3.10	3.084
5 C	3.12	3.1096			

The theoretical value of λg is obtained from the following relation[1]

$$\lambda g = \lambda_0 / [\epsilon_{r1} - x_1^2 (\lambda_0 / 2\pi a)^2]^{1/2} \qquad [1]$$

Where ϵ_{r1} is the dielectric constant of the rod ($\epsilon_{r1} = 2.56$) and x_1 is obt ained by solving the equations

$$x_1 \frac{J_0(x_1)}{J_1(x_1)} = x_2 \, \epsilon_{r1} \frac{H_0^{(1)}(x_2)}{H_1^{(1)}(x_2)} \qquad [2]$$

and $$x_1^2 + \left(\frac{x_2}{j}\right)^2 = \left(\frac{2\pi a}{\lambda_0}\right)^2 (\epsilon_{r1} - 1) \qquad [3]$$

where $x_1 = k_1' a, \quad x_2 = k_2' a$

and k_1', k_2' are related by the following equation

$$(k_1')^2 - (k_2')^2 = k^2 (\epsilon_{r1} - 1) \qquad [4]$$

where k is the free space wave number.

5. ANALYSIS OF RADIAL FIELD DECAY CURVES

The field distribution in the radial direction for some of the structures are shown in Figures 5 – 13. In order to determine whether the wave launched on the structure is a pure cylindrical surface wave, the follawing method[3] is used.

If ρ_1 and ρ_2 be two radii such that $\rho_1 \nless \rho_2$ and if the " identifying constant " $= n = \rho_2/\rho_1$ and the " Identifying ratio " is defined by

$$P_n(X_1) = \frac{H_1^{(1)}(j k_3 \rho_2)}{H_1^{(1)}(jk_3 \rho_2)} = \frac{H_1^{(1)}(X_2)}{H_1^{(1)}(X_1)} \qquad [5]$$

an identifying curve over any required range for a given range n is given by the plot $p_n(X_1)$ *Vs* X_1 (See Fig. 14).

The experimental decay curves (5-13) can be represented by functional relations, $f(\rho)$ *Vs* ρ. From the experimental field decay curves, the ratio $f(\rho_2)/f(\rho_1)$ is tabulated against ρ_1 for $n=2$. For a pure surface wave $f(\rho_2)/f(\rho_1) = p_n(X_1)$, so that from the identifying curve, if the corresponding values of X_1 are plotted against ρ_1, a straight line passing through the origin is expected. The linearity of this curve is a measure of the purity of the

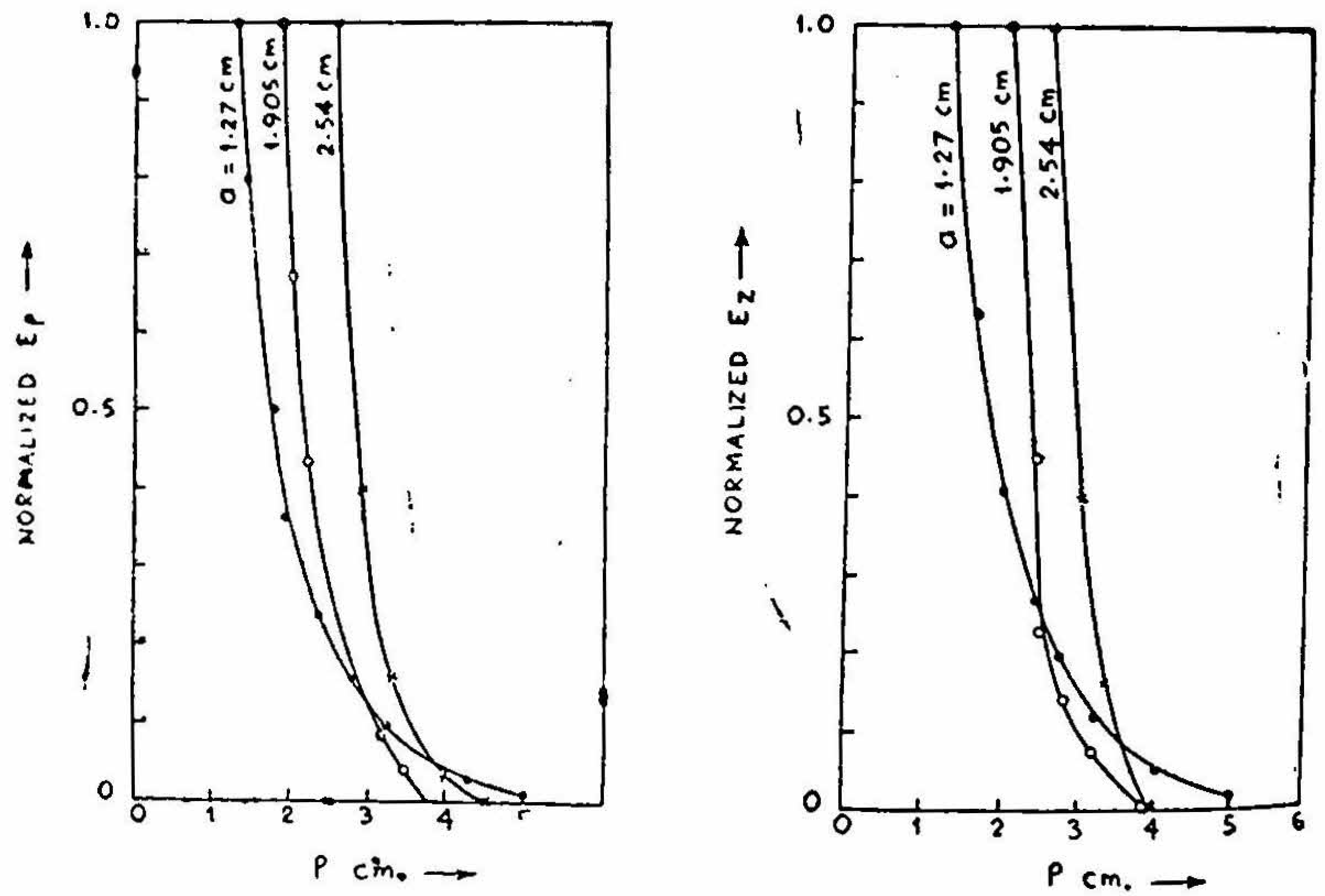

FIG. 5

Radial field decay curves (experimental) for uniform dielectric rod.

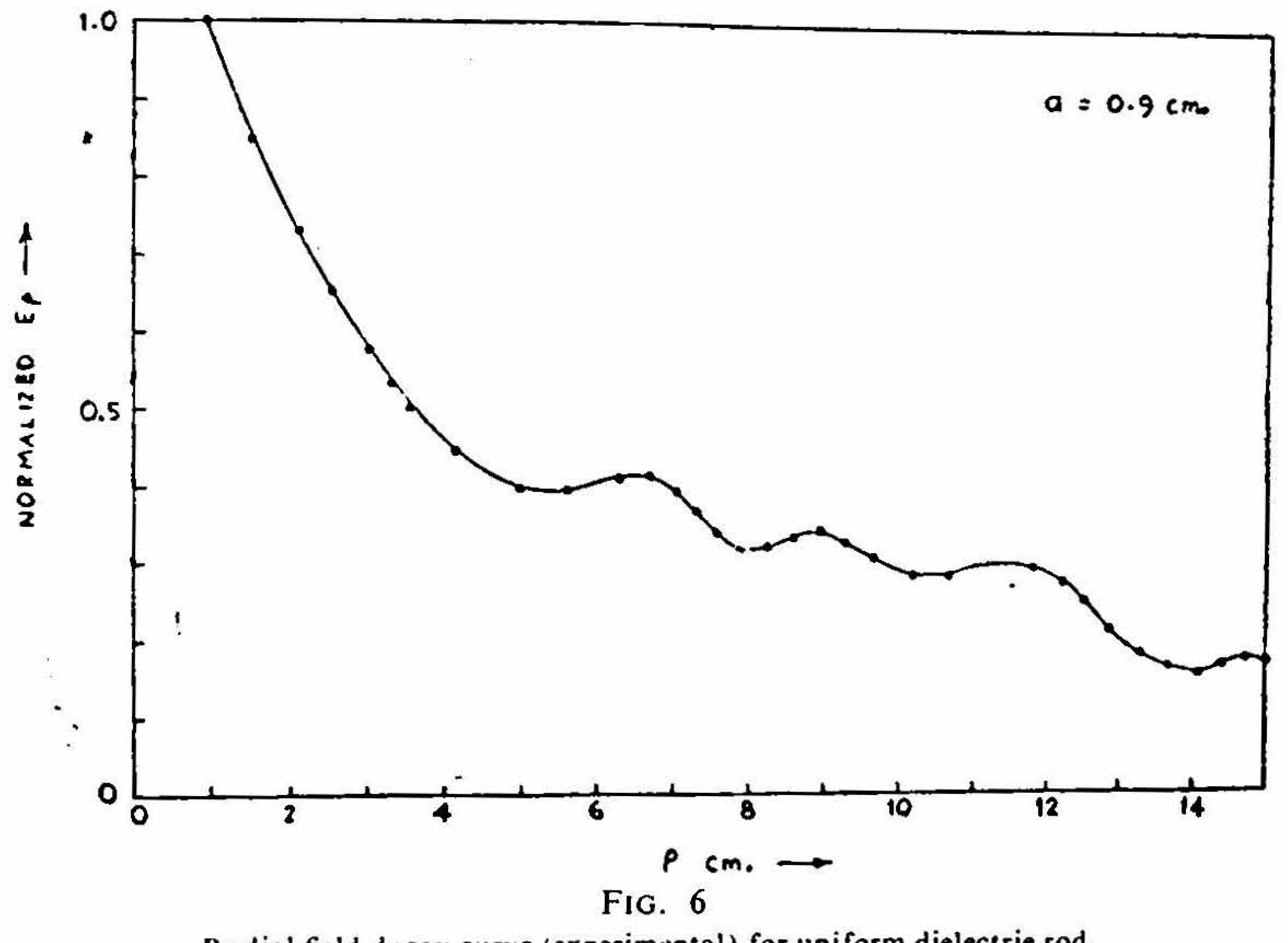

FIG. 6

Radial field decay curve (experimental) for uniform dielectrie rod.
a = Radius of the rod.

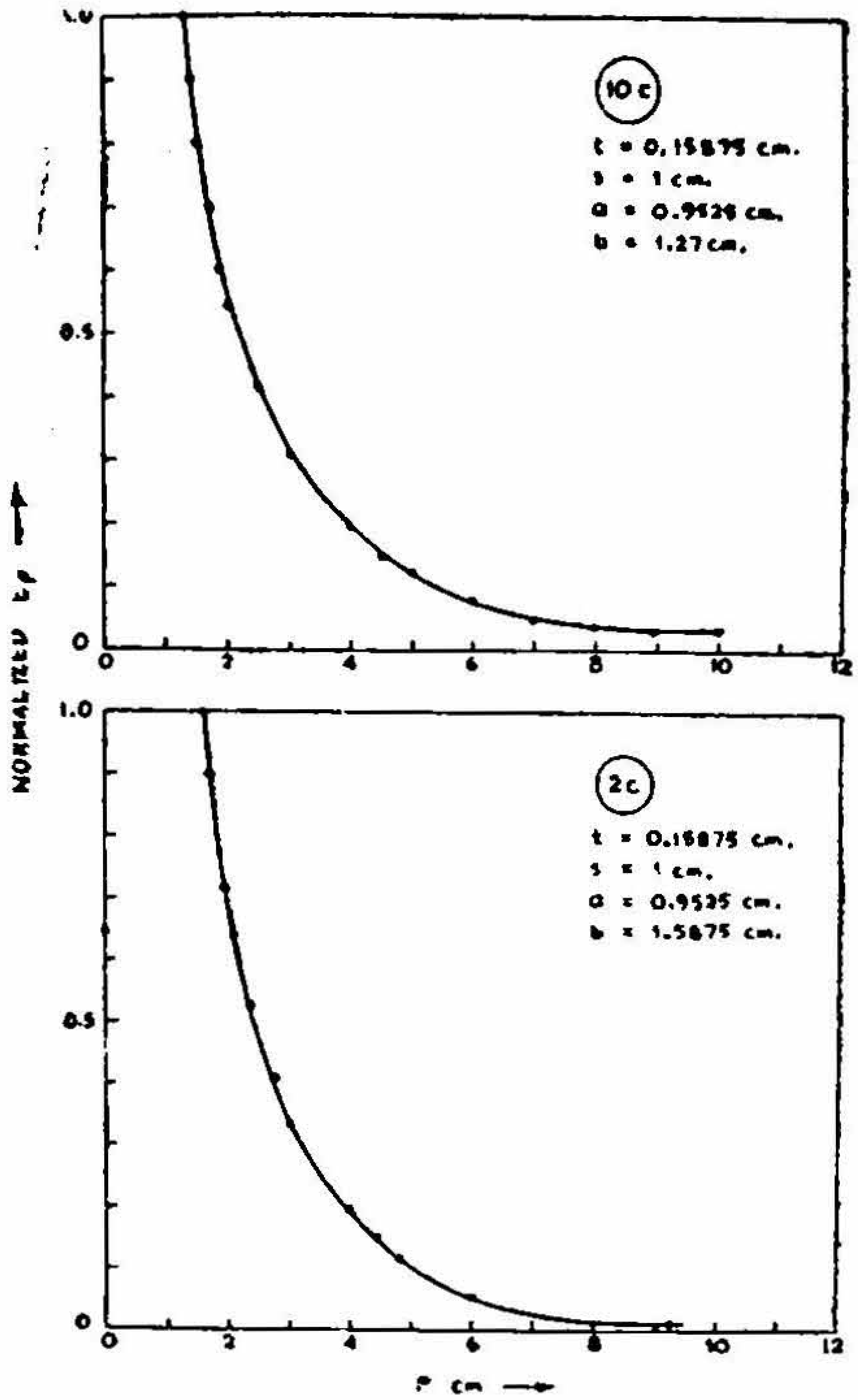

FIG. 7

Radial field decay curves (experimental) for corrugated dielectric rod.

t = Disc thickness a = Inner rod radius.

s = Disc spacing b = Disc radius.

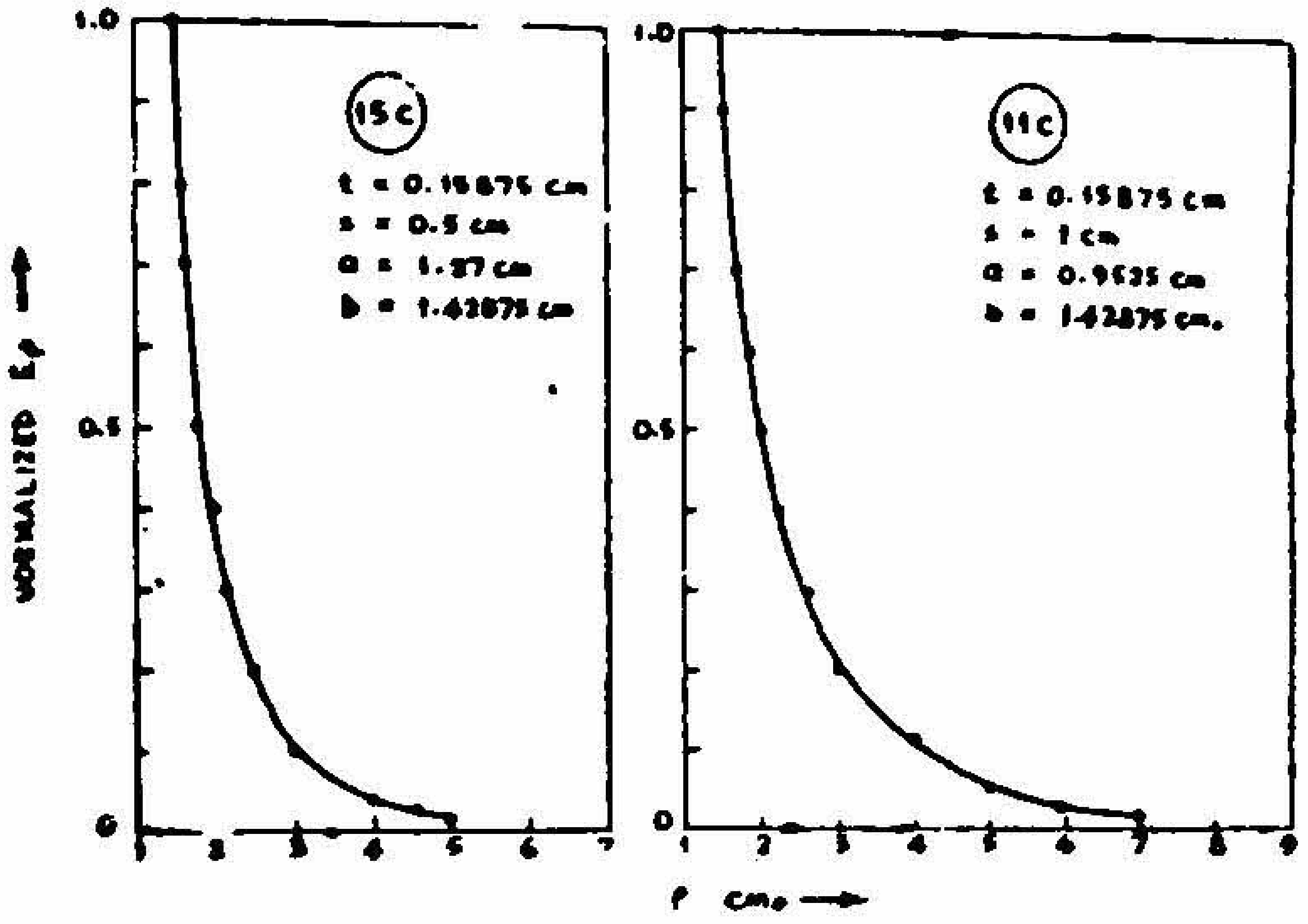

FIG 8.

Radial field decay curves (experimental) for corrugated dielectric rod.

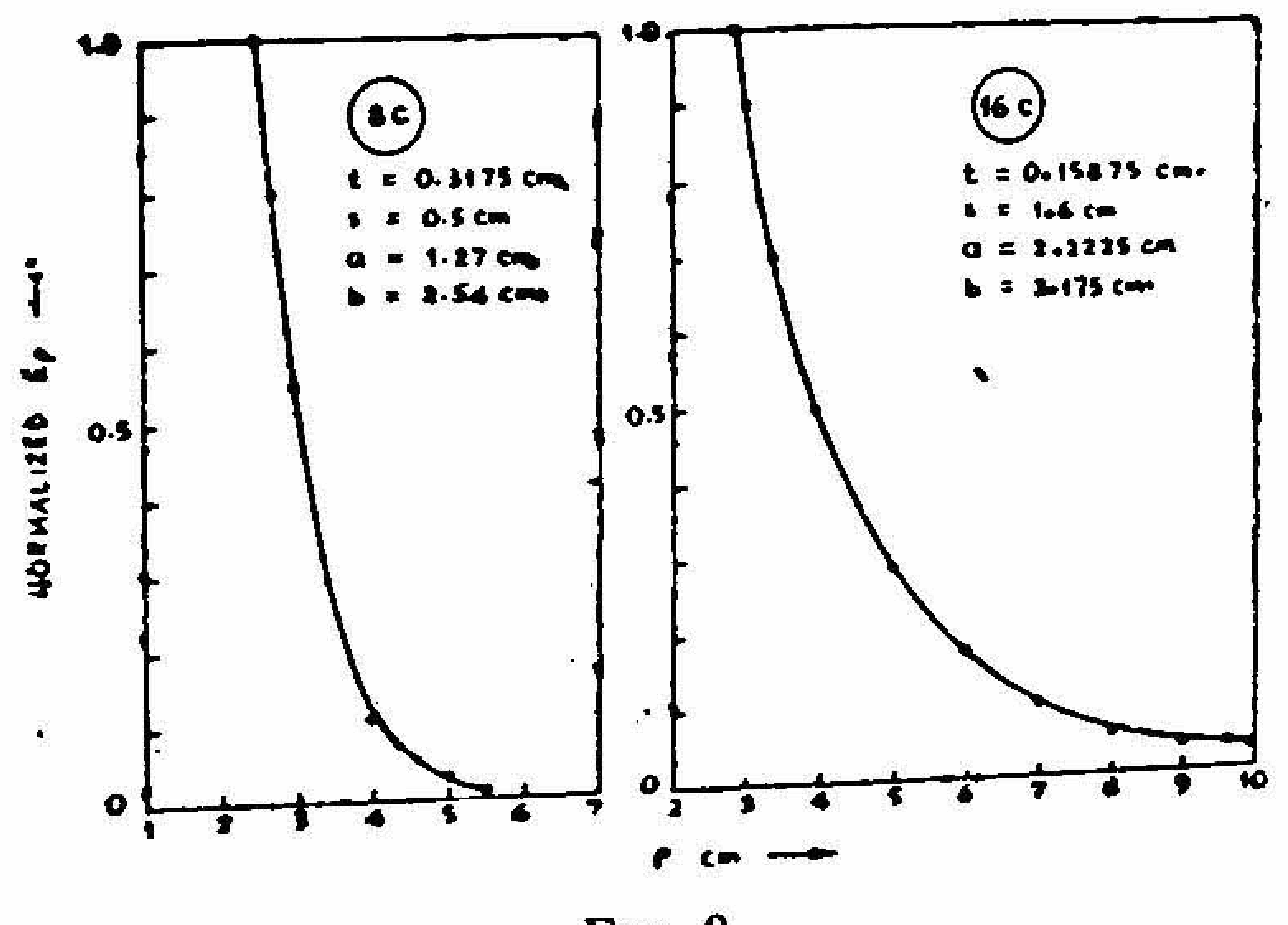

FIG. 9

Field decay curves (experimental) for corrugated dielectric rod.

t = Disc thickness **a = Inner rod radius.**

s = Disc spacing **b = Disc radius.**

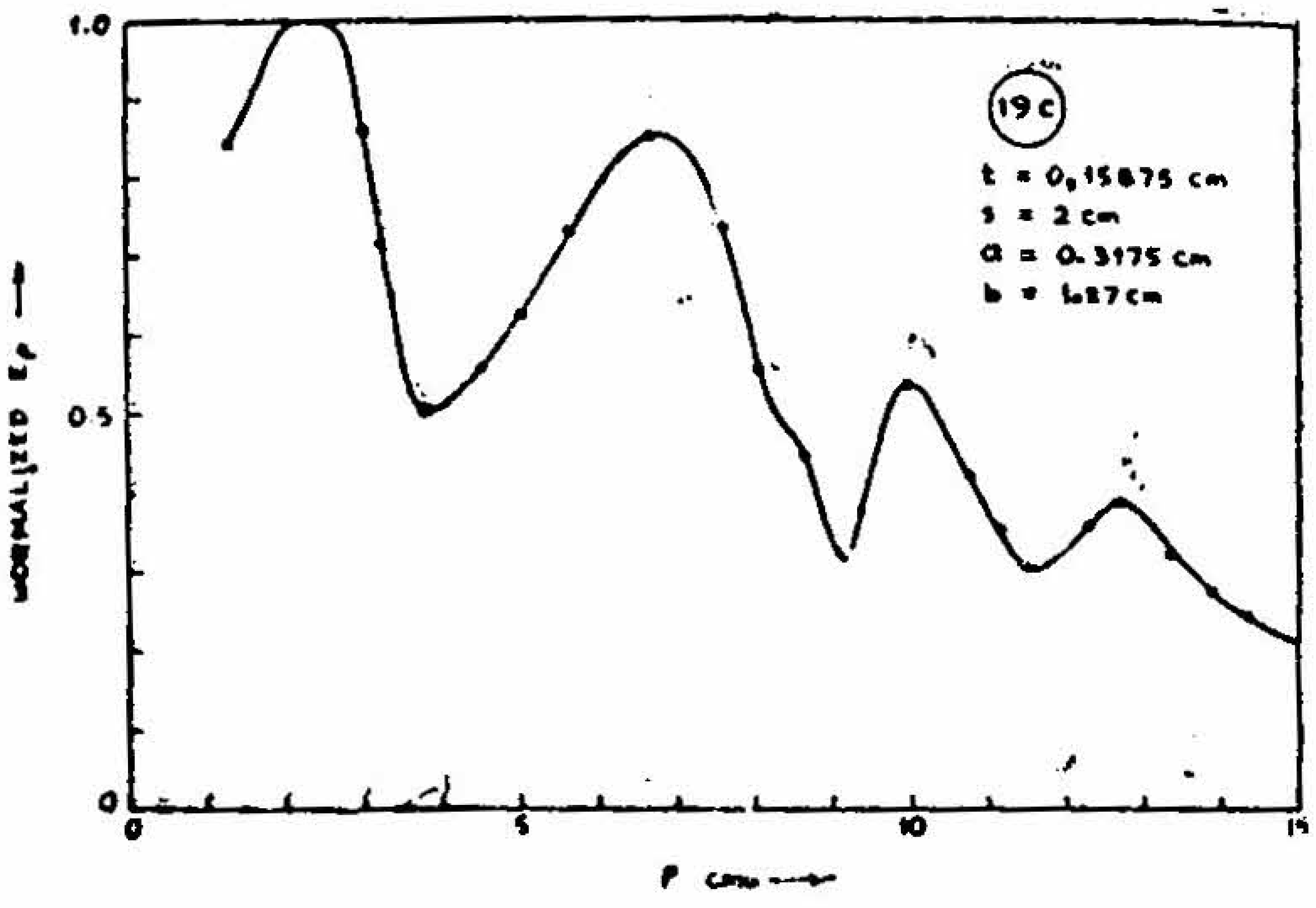

FIG. 10

Field decay curve (experimental) for corrugated dielectric rod.

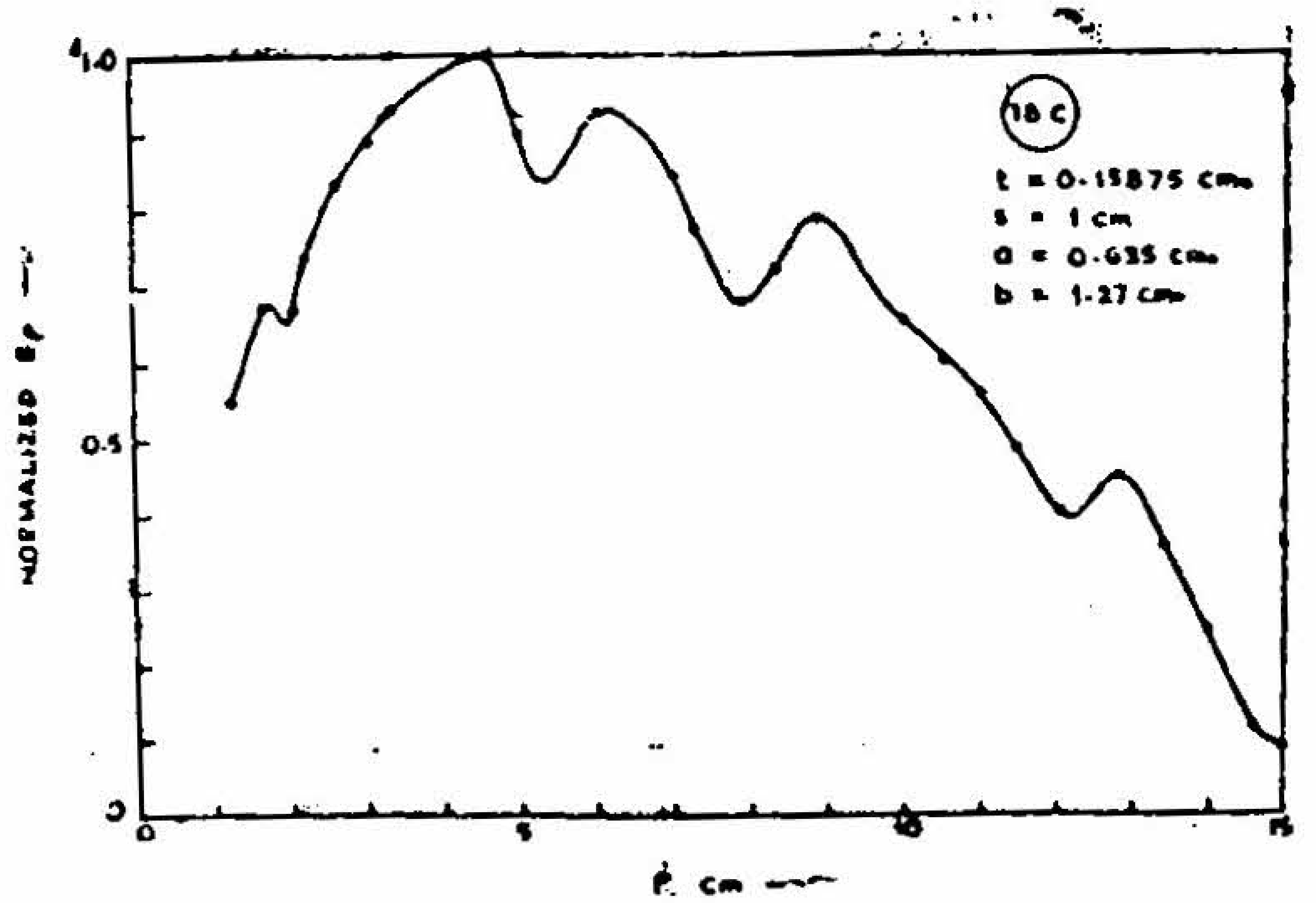

FIG. 11

Radial field decay curve (experimental) for corrugated dielectric rod.

t = Disc thickness a = Inner rod radius

s = Disc spacing b = Disc radius

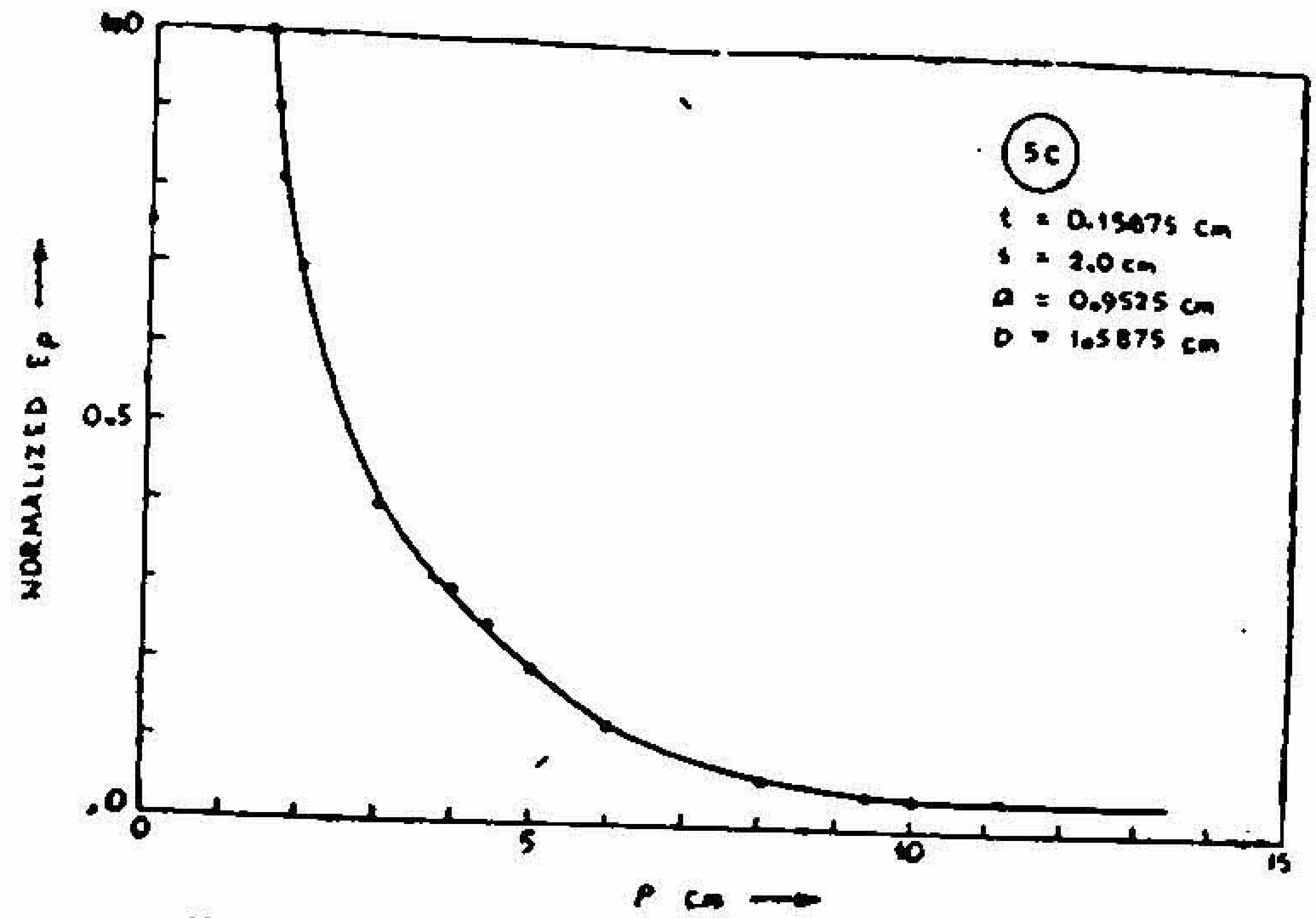

FIG. 12

Radial field decay curve (experimental) for corrugated dielectric rod.

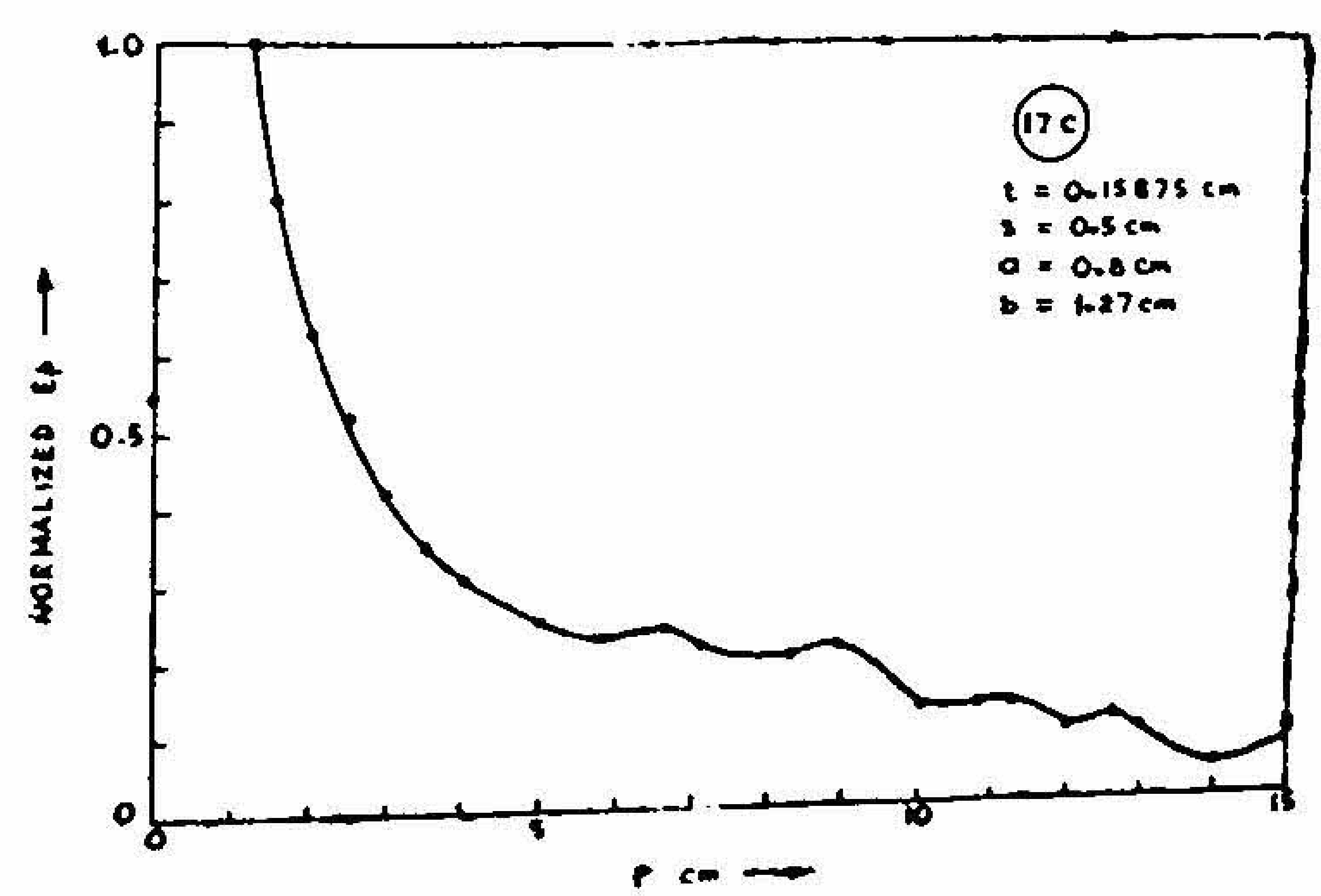

FIG. 13

Field decay curve (experimental) for corrugated dielectric rod.

t – Disc thickness a – Inner rod radius

s – Disc spacing b – Disc radius

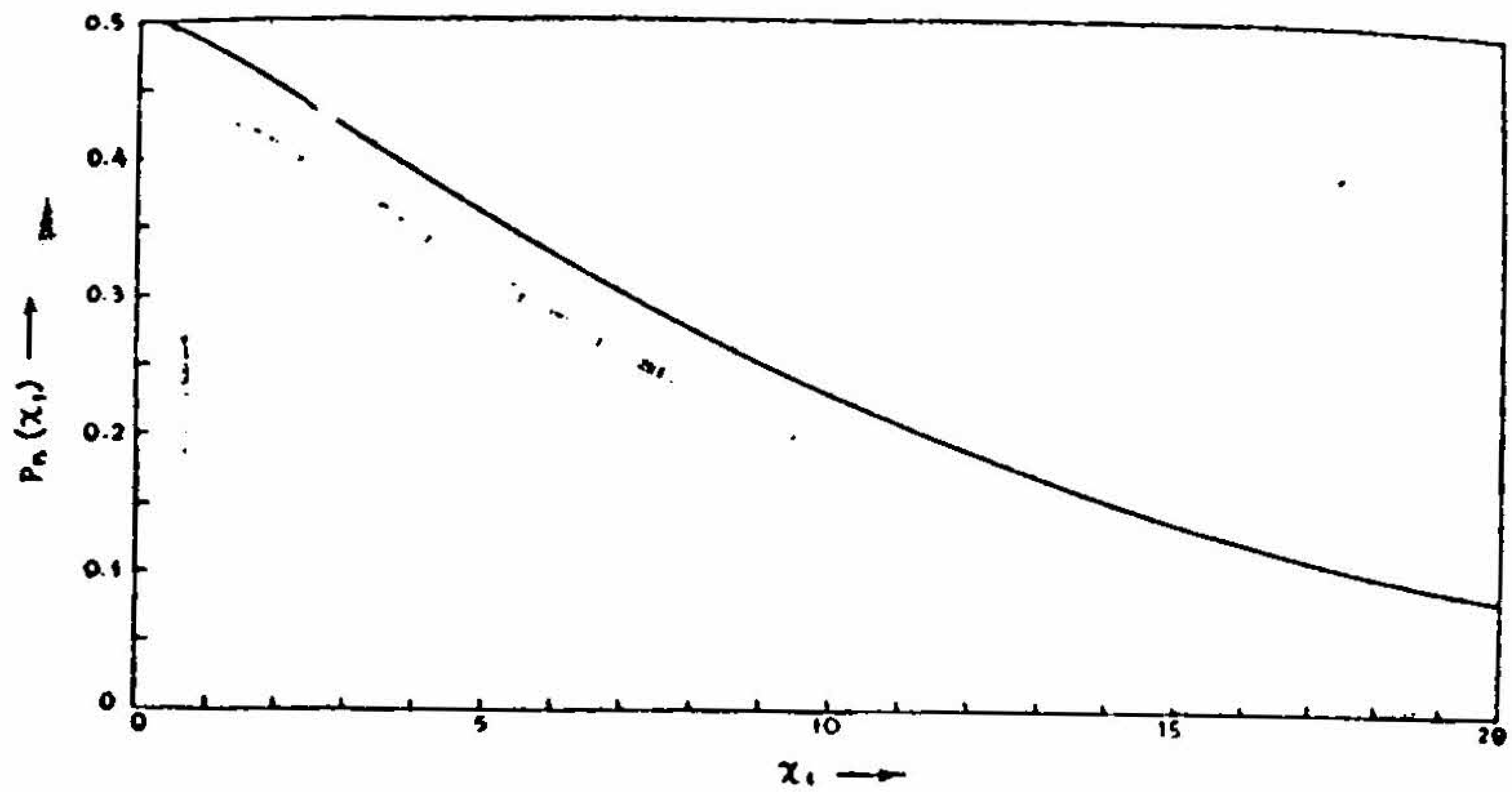

FIG. 14

Identifying curve for $H_1^{(1)}(X)$.

Identifying ratio $P_n=(X_1)=\frac{H_1^{(1)}(jkp_2)}{H_1^{(1)}(jkp_1)}$

Identifying constant $n=P_2/P_1=2$

surface wave and the slope of the curve gives the value of decay coefficient $\xi=k_3$. Fig. 15 shows the identifying lines for some of the experimental field decay curves. The experimental decay coefficients obtained by the above method are compared with theoretical values in Table 2.

TABLE 2

Measured and Theoretical values of Decay Coefficient

Structure Number	Measured values of ξ cm^{-1}	Theoretical Values of ξ cm^{-1}	Structure Number	Measured values of ξ cm^{-1}	Theoretical values of ξ cm^{-1}
1 u	.82	0 826	6 C	1.05	1.044
7 u	.978	0 978	4 C	1.185	1.185
8 u	1.185	1 417	8 C	1 42	1.406
9 u	1.72	1.738	9 C	0.13	0.158
10 u	1 858	1.938	10 C	0.28	0.283
11 u	2 04	2 067	11 C	0.55	0.578
12 u	2.11	2 159	12 C	0.50	0.517
1 C	0 66	0.674	13 C	0.54	0.578
2 C	0 40	0.425	14 C	0.40	0.395
3 C	0.36	0.3 6	15 C	1.102	1.035
4 C	0 33	0.33	16 C	0.40	0 3823
5 C	0.20	0.279			

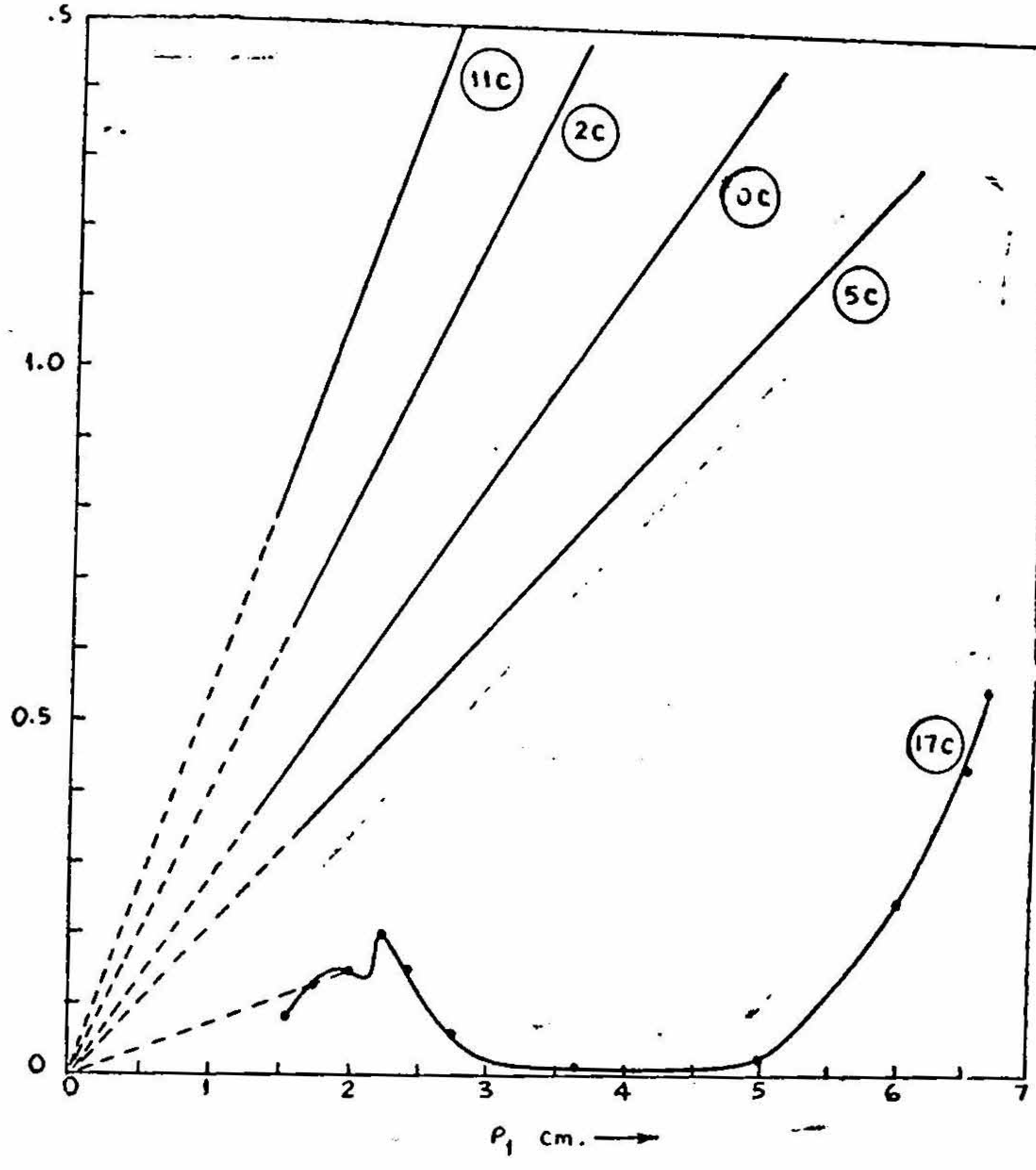

FIG. 15
Identifying lines.

	11*C*	2*C*	10*C*	5*C*	17*C*
t	1.15875 cm	0.15875 cm	0.15875 cm	0.1875 cm	0.15875 cm
s	1.0 cm	1.0 cm	1.0 cm	2 0 cm	0.5 cm
a	0 9525 cm	0.9525 cm	0.9525 cm	0 9525 cm	0.8 cm
b	1.42875 cm	1.5875 cm	1.27 cm	1.5875 em	1.27 cm
Measured Slope	0 55 cm^{-1}	0.40 cm^{-1}	0 28 cm^{-1}	0.21 cm^{-1}	Does not support a pure surface wave.

t = Disc thickness *a* = Inner rod radius.
s = Disc spacing *b* = Disc radius.

The field decay curve (Fig. 6) shows that a uniform dielectric rod whose radius is below cut-off value cannot support a pure surface wave. The field decay curves for corrugated rods shows that (See Figures 10 and 11) the the structures 10 and 11 cannot support pure surface wave which is confirmed by theory[1]. The structures which support pure surface waves have their identifying lines straight.

6. MEASUREMENT OF ATTENUATION CONSTANT

The v.s.w.r. is measured close to the surface of the guiding structure with the aid of a probe. The attenuation constant α is calculated from the relation

$$\alpha = (1/l) \text{ arc tanh } (\text{v.s.w.r.})^{-1} \qquad [b]$$

where l, is the length of the structure measured from the point where the v.s.w.r. is measured to the end of the structure. The v.s.w.r. is measured at different distances from the feed end and the average values are reported in Table 6.

7. MEASUREMENT AND ANALYSIS OF RADIATION PATTERNS

The experimental set-up for radiation measurement is shown in Fig. 16. Some of the theoretical and experimental radiation patterns for uniform and corrugated aerials are shown in Figures 17–25. The analysis of radiation pattern shows that (*a*) most of the measured patterns show better agreement with the theory derived by considering radiation from both the end as well as the surface of the structure. (*b*) measured beam width, position of lobes agree fairly well with the theory. The theoretical radiation are calculated from[2] the following relations.

(*a*) Uniform Rod : Field Pattern

Case A t Considering radiations from the surface only.

$$E_{PS} = \left[B \frac{1}{2r} \left(\frac{\mu_0}{\epsilon_0} \right)^{1/2} k k_1' L a J_1 (k_1' a) \right] \times$$
$$\left[\exp j(\omega t - kr) \exp \left(-j \frac{L}{2} (\beta - k \cos \theta) \right) \right] \times$$
$$\left[\frac{\sin x}{x} \right] [J_0 (ka \sin \theta) \sin \theta - C J_1 (ka \sin \theta)) \qquad [7]$$

$$x = \frac{1}{2} (\beta - k \cos \theta)$$

$$C = \frac{k_1' J_0 (k_1' a)}{\epsilon_{r1} k J_1 (k_1' a)}$$

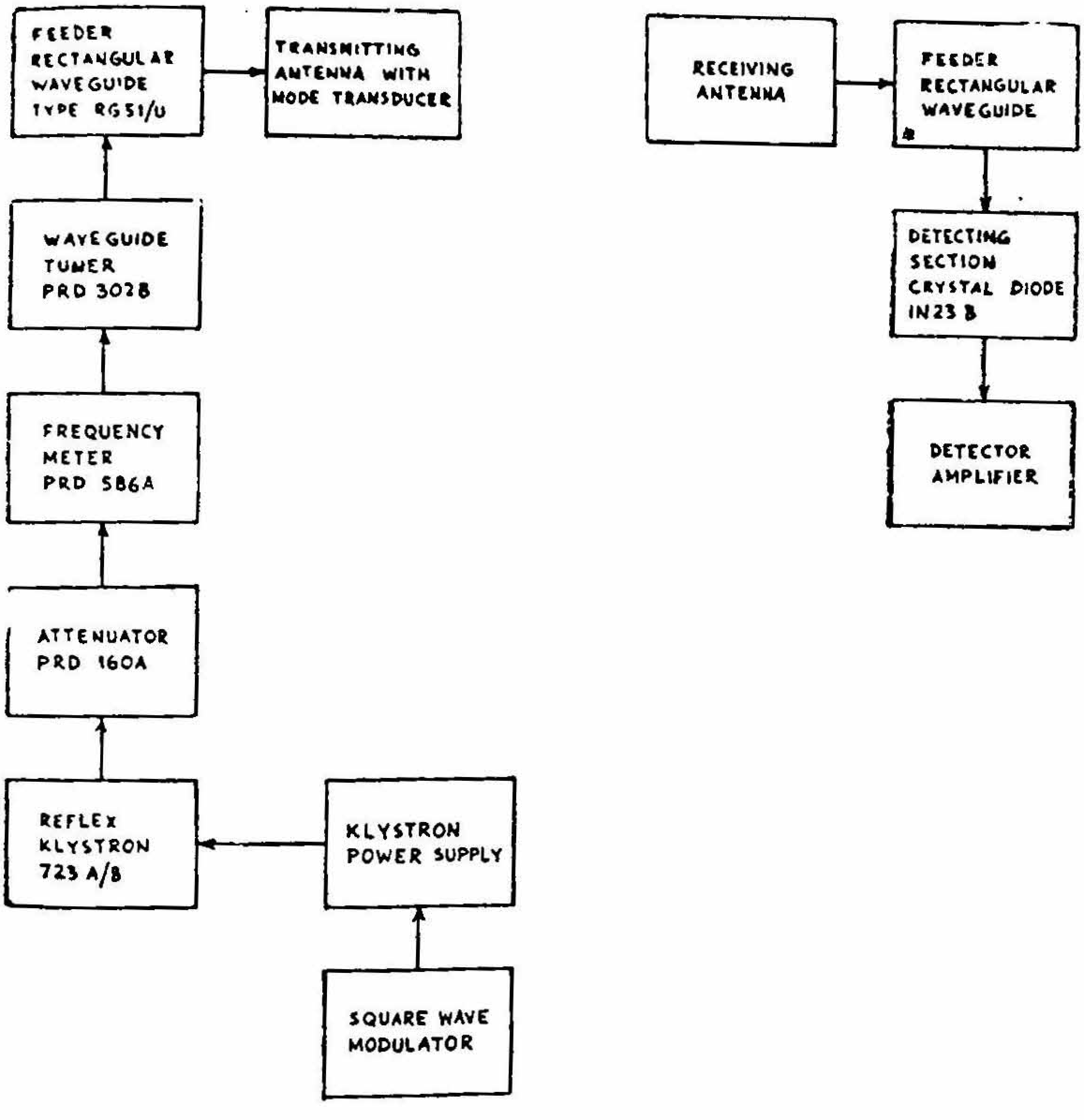

FIG. 16

Block diagram of experimental set up used for radiation pattern measurement.

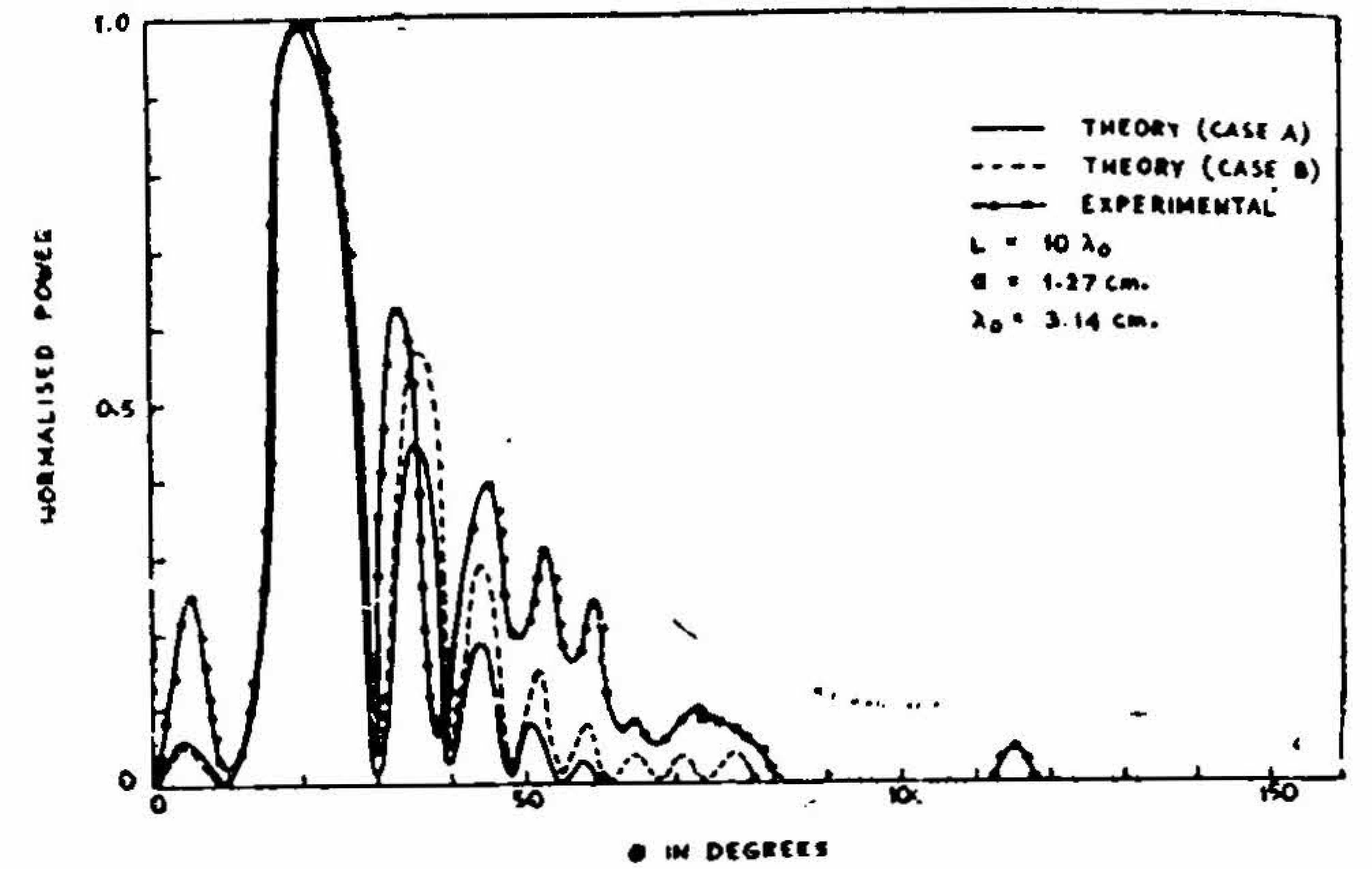

FIG. 17

Ratiation pattern (power) for unlform dielectric rod.
L = Length of the rod, a = Radius of the rod.

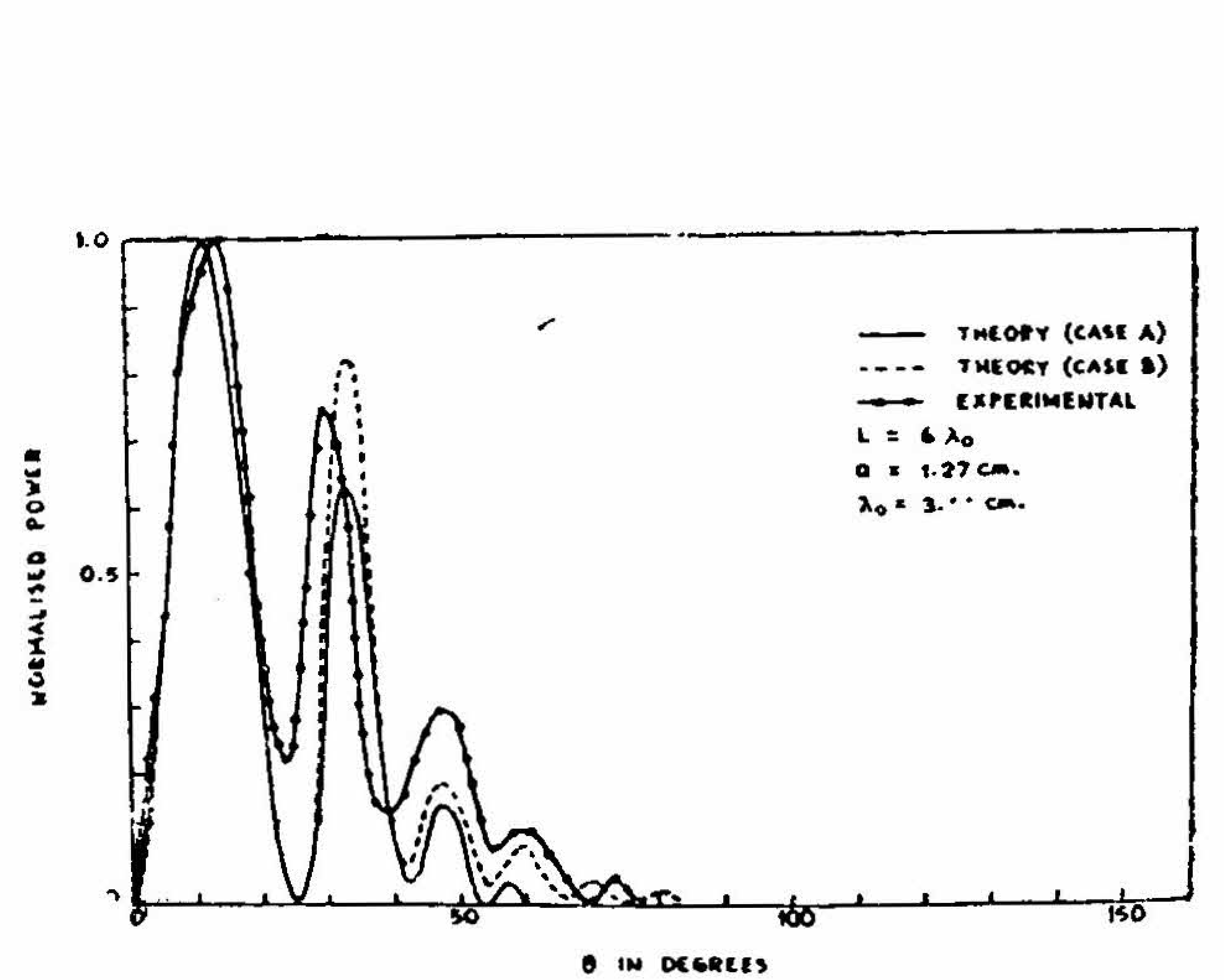

FIG. 18

Radiation pattern (power) for uniform dielectric rod.
L = Length of the rod, a = Radius of the rod.

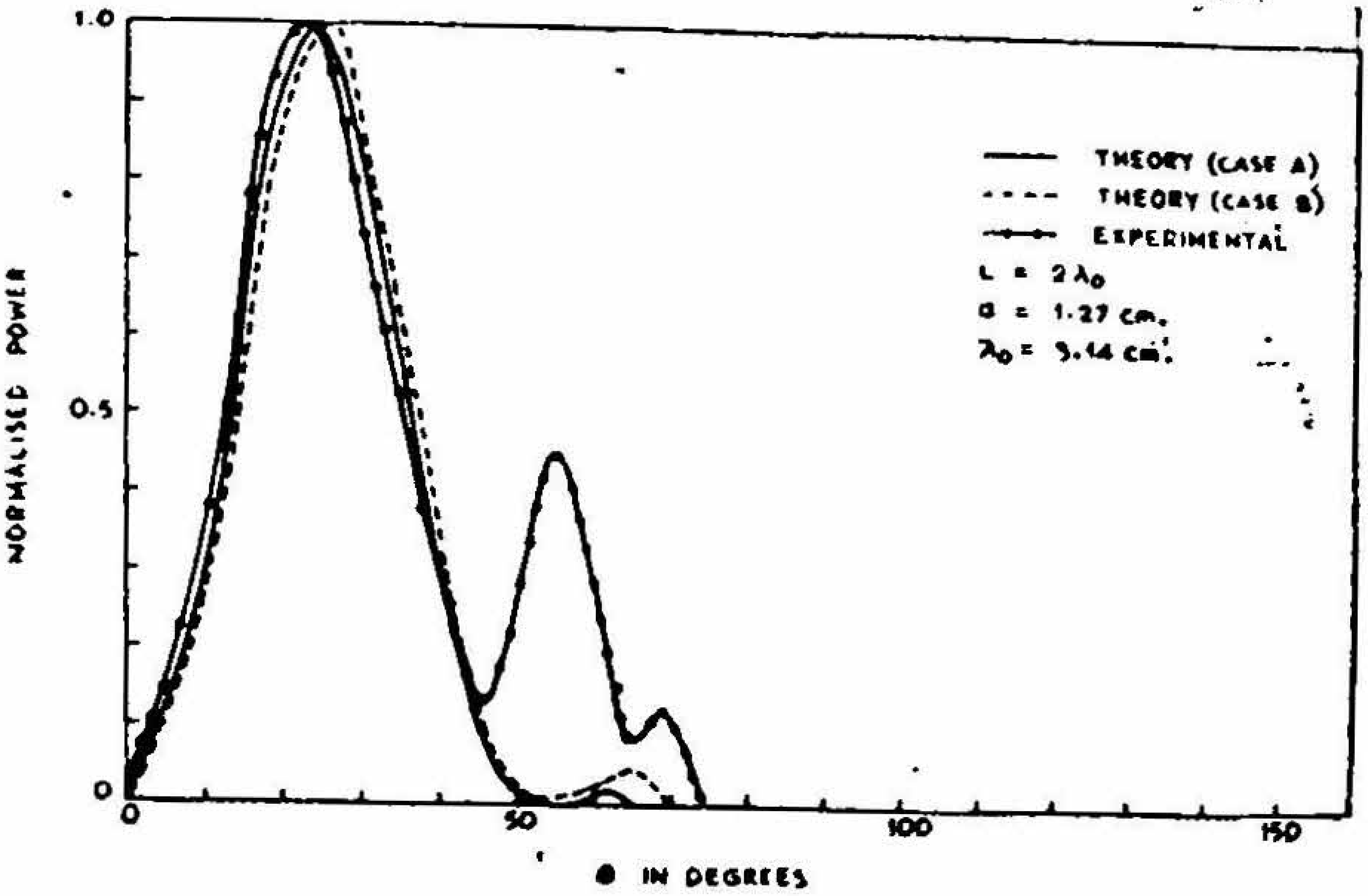

FIG. 19

Radiation pattern (power) for uaiform dielectric rod. L=Length of the rod, a=Radius of the rod.

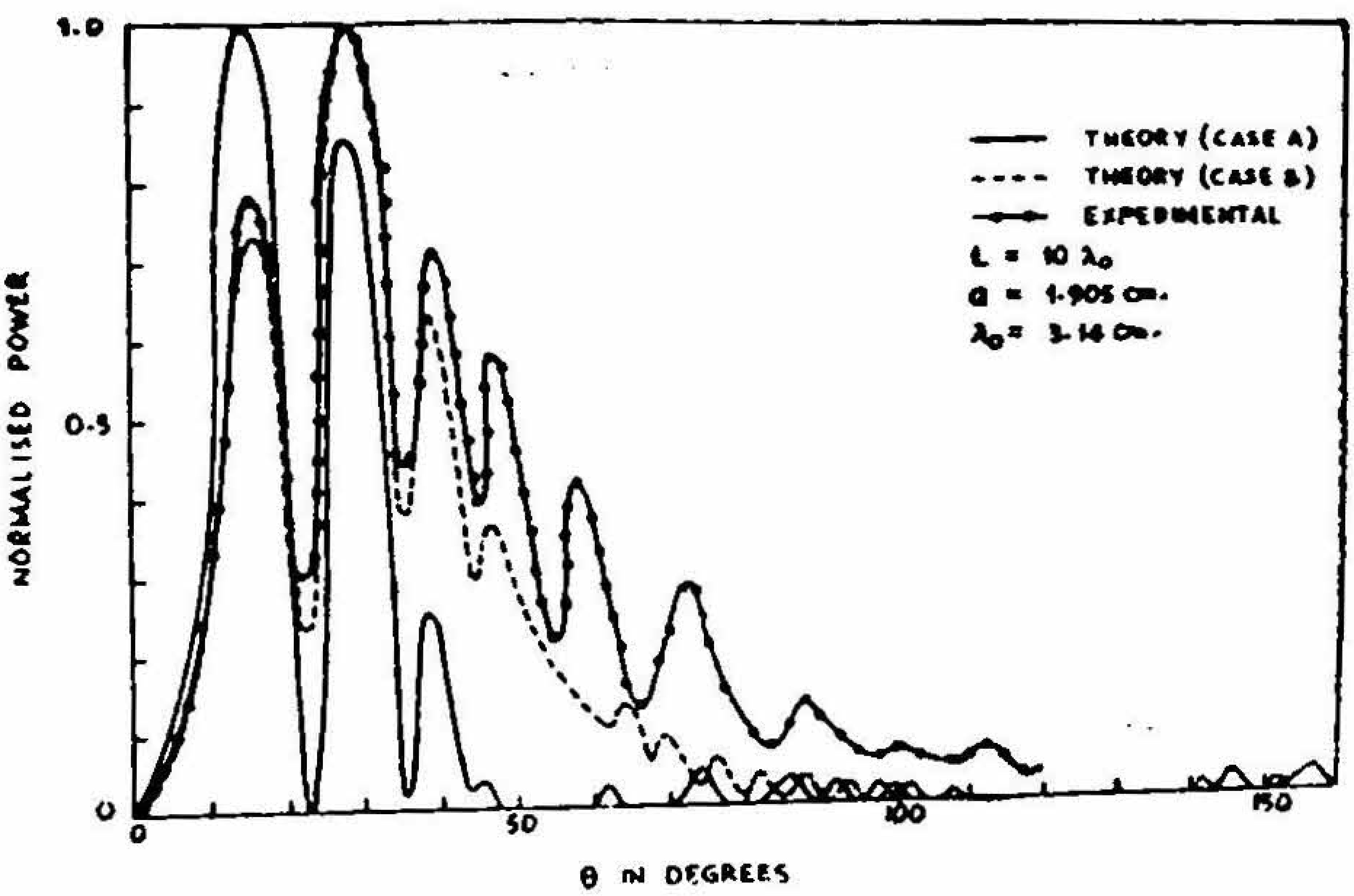

FIG. 20

Radiation pattern (power) for uniform dielectric rod. L=Length of the rod, a=Radius of the rod.

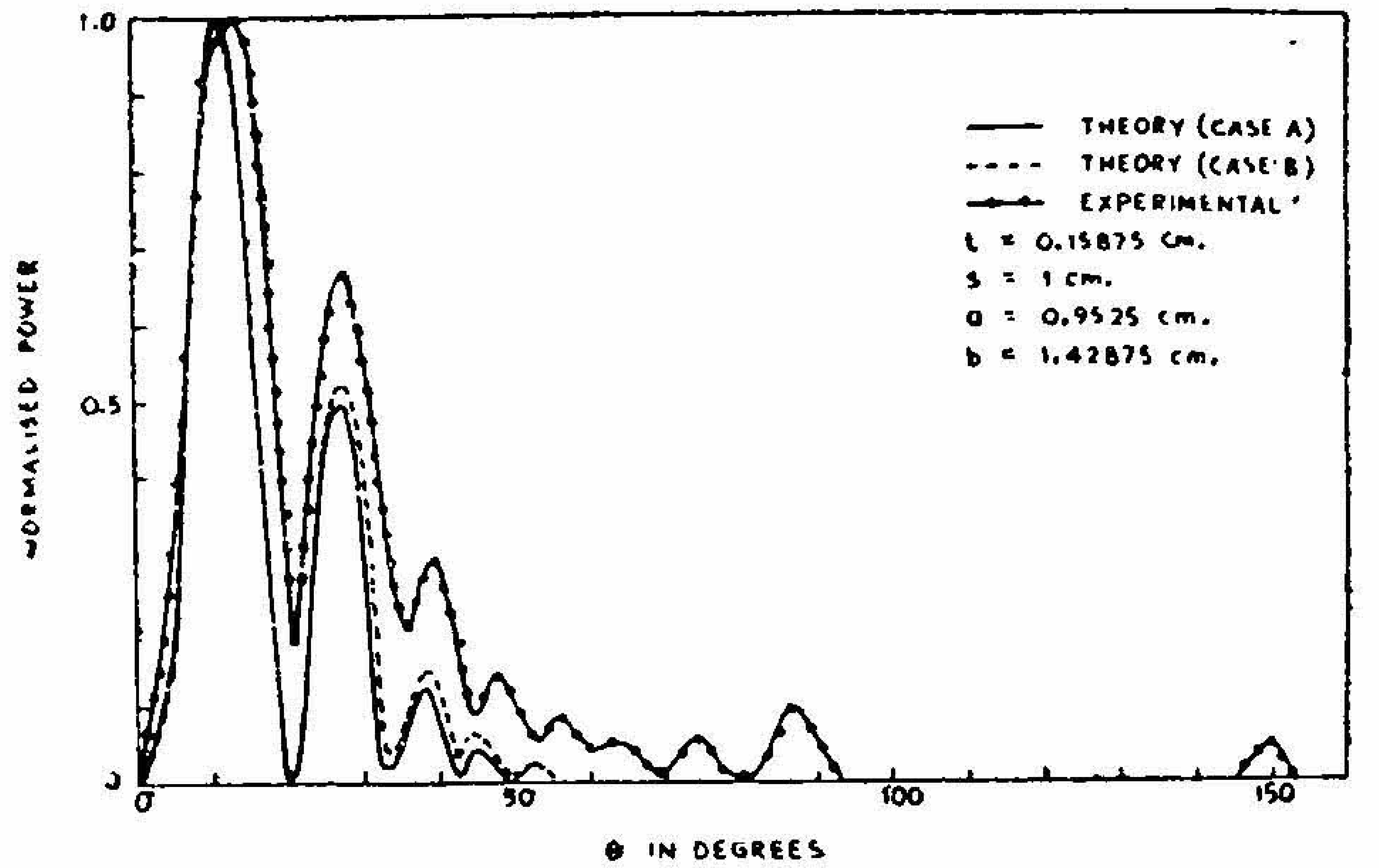

FIG. 21

Radiation pattern (power) for corrugated dielectric dielectric rod.
t=Disc thickness a=Inner rod radius.
s=Disc spacing b=Disc radius.

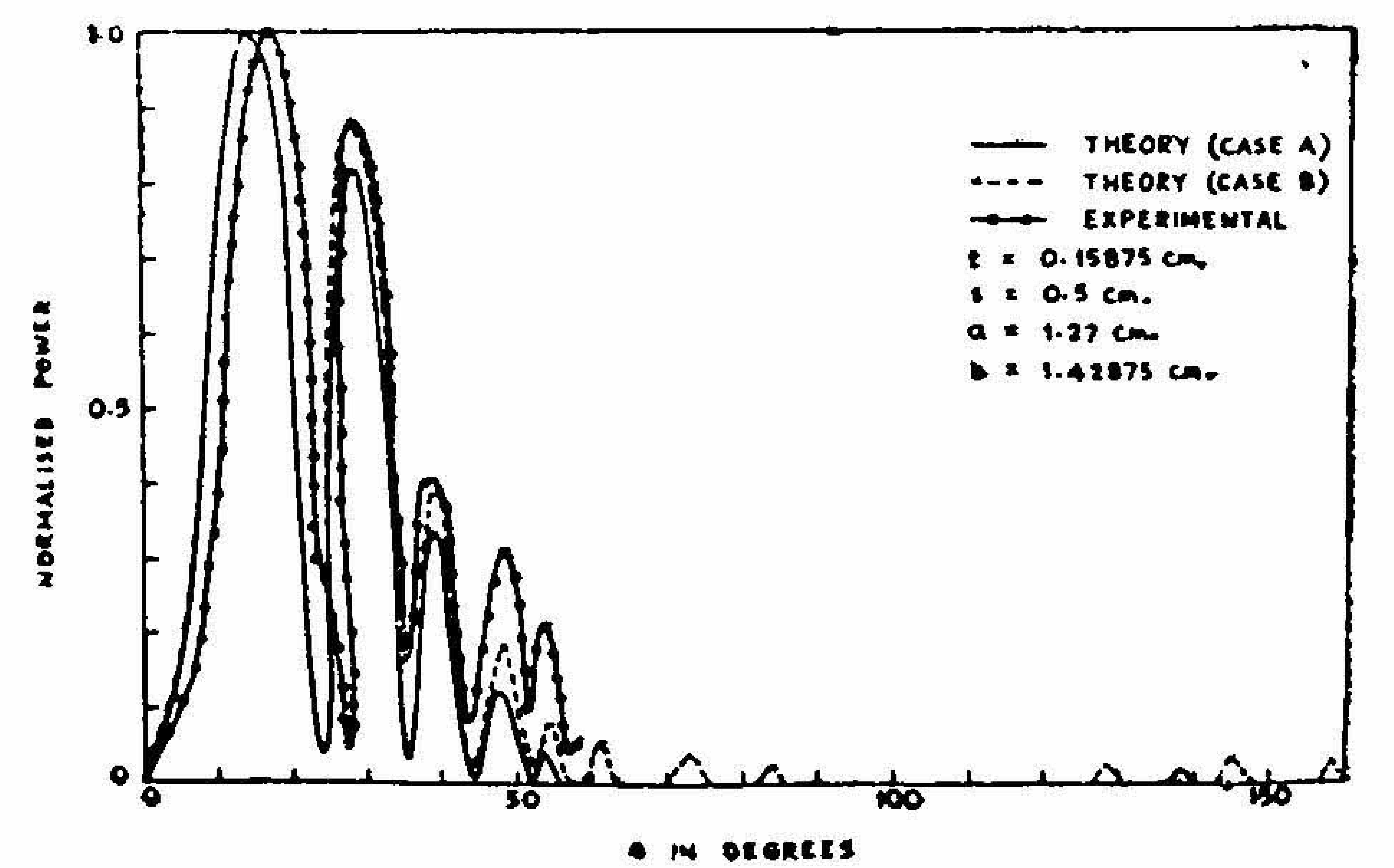

FIG. 22

Radiation pattern (power) for corrrgated dielectric rod.
t=Disc thickness a=Inner rod radius.
s=Disc spacing b=Disc radius.

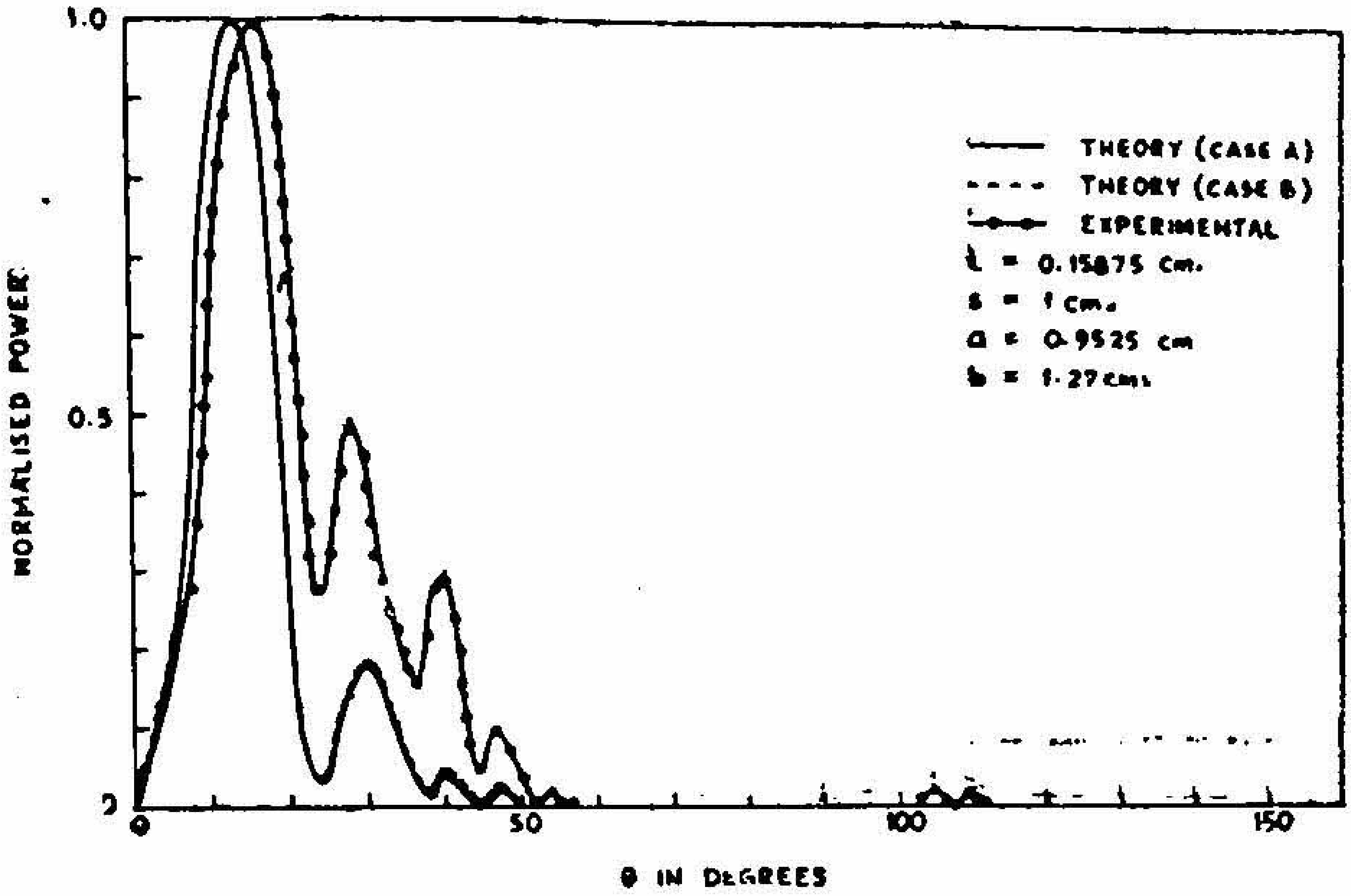

Fig. 23

Radiation pattern (power for corrugated dielectric rod.
t = Disc thickness a = Inner rod radius.
s = Disc spacing b = Disc radius.

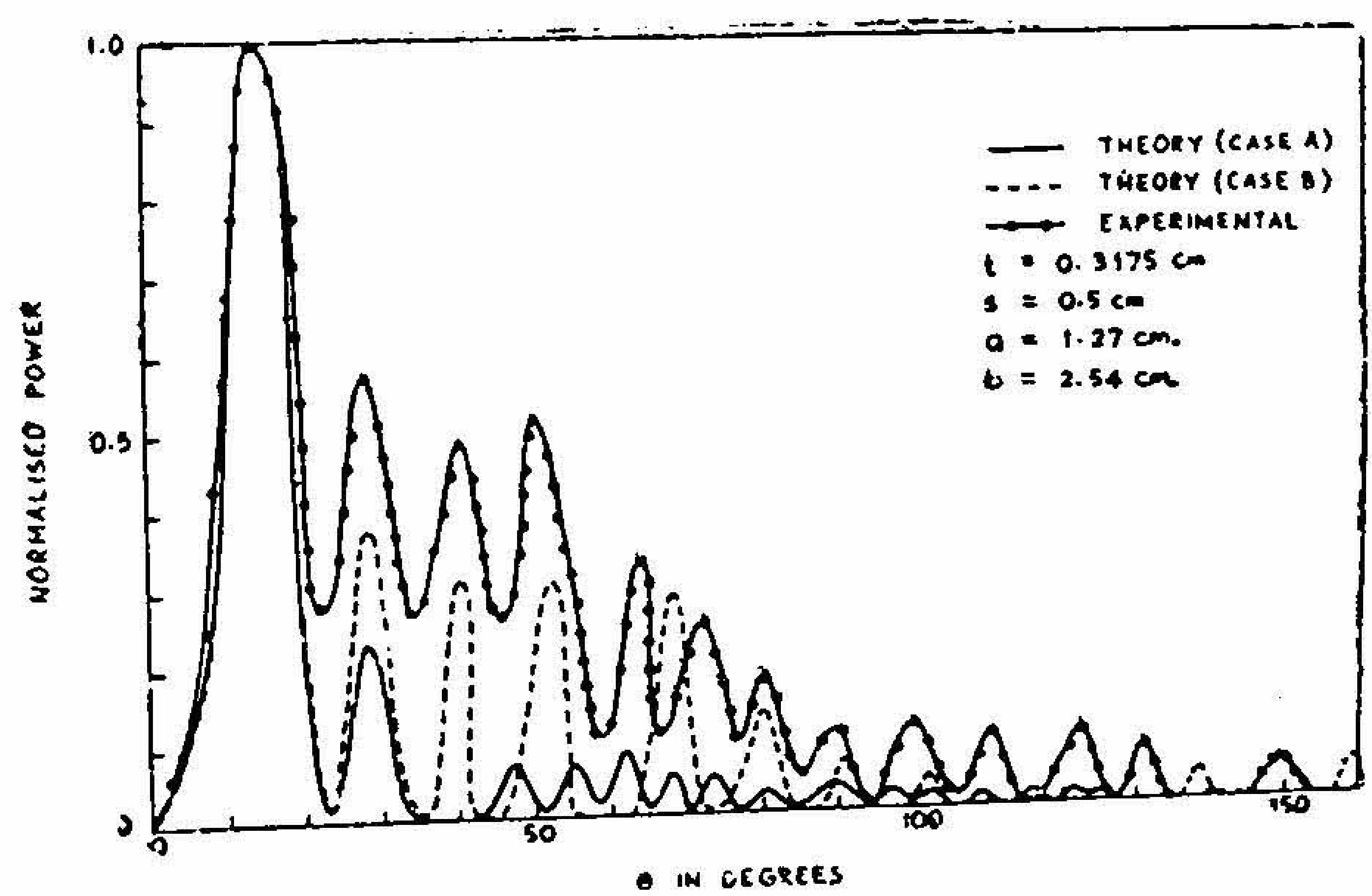

Fig. 24

Radion pattern (power) for corrugated dielectric rod.
t = Disc thickness a = Inner rod radius.
s = Disc spacing b = Disc radius.

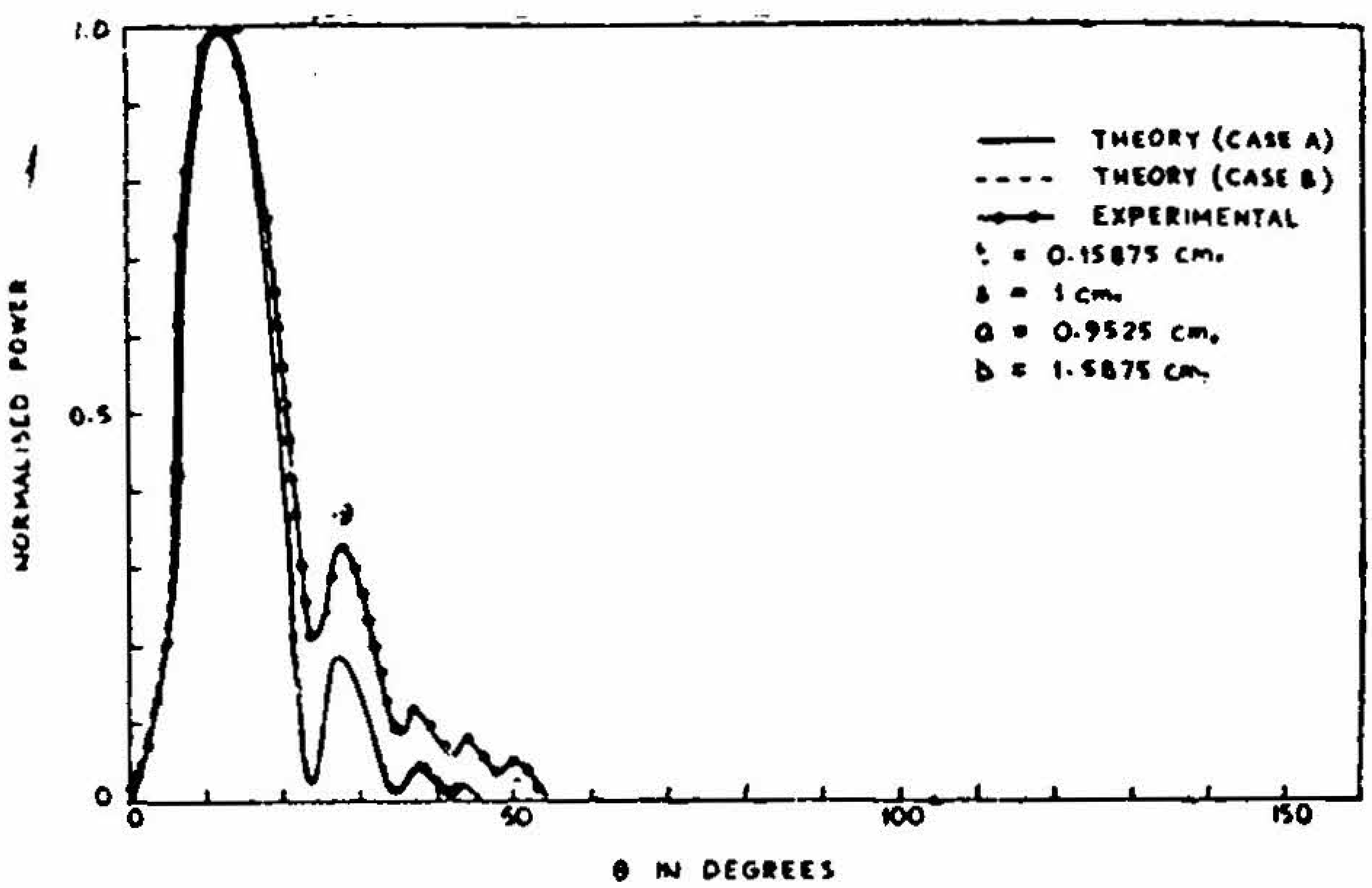

FIG. 25

Radiation pattern (power) for corrugated dielectric rod.
t=Disc thickness a=Inner rod radius.
s=Disc spacing b=Disc radius.

Case B: Codsidering radiation from the surface as well as end.

$$|E_p| = [(A')^2 + (B')^2 + 2\,A'\,B'\,\sin x]^{1/2} \qquad [8]$$

$$A' = [(B/2r)\,(\mu_0/\epsilon_0)^{1/2}\,k\,k_1'\,L\,a\,J_1(k_1'\,a)] \times$$

$$\left[\frac{\sin x}{x}\right] J_0(ka\sin\theta)\sin\theta - C\,J_1(ka\sin\theta)]$$

$$B' = \left[\frac{B\,(\mu_0/\epsilon_0)^{1/2}\,k\,l_1'\,a\,J_1\,(k_1'\,a)}{2\,r}\right] \times$$

$$\left[\left\{k\cos\theta + \frac{\beta}{r'}\right\}\right]\left[\frac{J_0(ka\sin\theta)\sin\theta - D\,\epsilon_{r1}\,J_1(ka\sin\theta)}{(k_1')^2 - (k\sin\theta)^2}\right.$$

(*b*) Corrugated Rod : Field Pattern.

Case A : Surface Radiation only

$$E_{PS}^{\cdot} = \left[-\frac{1}{2r} \frac{b\,L\,k^2\,\epsilon_{r2}}{k_2} \{A_2\,J_1(k_2\,b) + A_3\,Y_1(k_2\,b)\} \right] \times$$

$$\exp\left[-j\,\frac{L}{2}\,(\beta - k\,\cos\theta) \right] \times$$

$$[J_0(kb\,\sin\theta)\,\sin\theta - C''\,J_1(kb\,\sin\theta)]\left[\frac{\sin x}{x}\right] \tag{9}$$

$$C'' = \frac{k_2}{k\epsilon_{r2}} \frac{A_2\,J_0(k_2\,b) + A_3\,Y_0(k_2\,b)}{A_2\,J_1(k_2\,b) + A_3\,Y_1(k_2\,b)}$$

Case B : Surface and End Radiation.

$$|E_P| = [(A'')^2 + (B'')^2 + 2A''\,B''\,\sin x]^{1/2} \tag{10}$$

$$A'' = \left[\frac{A_2}{2r} \left(\frac{b\,L\,k^2\,\epsilon_{r2}}{k_2} \right) \left(J_1\,(k_2\,b) + \frac{A_3}{A_2}\,Y_1(k_2\,b) \right) \right] \times$$

$$\left[J_0(kb\,\sin\theta)\,\sin\theta - \frac{k_2}{k\epsilon_{r2}} \left\{ \frac{J_0(k_2\,b) + (A_3/A_2)\,Y_0(k_2\,b)}{J_1(k_2\,b) + (A_3/A_2)\,Y_1(k_2\,b)} \right\} J_1(kb\,\sin\theta) \right] \times$$

$$\left[\frac{\sin x}{x} \right]$$

$$B'' = \left[A_2\,\frac{A_1}{A_2}\,\frac{ka}{k_1}\,(k\,\epsilon_{r1}\,\cos\theta + \beta) \right] \times$$

$$\left[\frac{k_1\,J_1(ka\,\sin\theta)\,J_0(k_1\,a) - k\,\sin\theta\,J_1(k_1\,a)\,J_0(ka\,\sin\theta)}{k_1^2 - (k\,\sin\theta)^2} \right]$$

$$\frac{A_3}{A_2} = \frac{(k_3/k_2)\,\epsilon_{r2}\,[H_0^{(1)}\,(k_3 b)/H_1^{(1)}\,(k_3\,b)]\,J_1(k_2\,b) - J_0\,(k_2\,b)}{Y_0(k_2\,b) - (k_3\,\epsilon_{r2}/k_2)\,[H_0^{(1)}\,(k_3\,b)/H_1^{(1)}\,(k_3\,b)]\,Y_1(k_2 b)}$$

$$\frac{A_1}{A_2} = \frac{J_0(k_2\,a) + (k_3\,\epsilon_{r2}/k_2)\,[H_0^{(1)}\,(k_3\,b)/H_1^{(1)}\,(k_3\,b)]\,Y_0(k_2\,a)}{J_0(k_1\,a)}$$

8. MEASUREMENT OF GAIN

The gain of aerials has been measured by comparison method. The aerial 10 C ($t=0.15875$ cm, $s=1$ cm, $a=0.9525$ cm and $b=1.27$ cm) which is found to have the highest gain is used as a reference aerial. It is to be noted that in finding the gain of the reference aerial by comparison with a phyramidal horn, the power input to the horn which is directly fed from the rectangular guide is different from the power input fed to the aerial 10 C from the mode transducer. The gain of the test aerial (10 C) is calculated in the following way

$$G=G_1 \frac{P_1}{P_2}=\frac{W_2}{W_1}\frac{P_1}{P_2} G_H \quad [7]$$

where, W_1 and W_2 are the relative power levels when the pyramidal horn and the test antenna are used as transmitting aerials, which correspond to microammeter readings in the two cases

$$\left.\begin{array}{l} W_1=1000\ \mu A \\ W_2'=350\ \mu A \end{array}\right\} \text{measured values}$$
$$G_H=20\ db=100$$

P_1 and P_2 correspond to the relative input power levels in the two cases which are proportional to the respective launching efficiencies.

The launching efficiency of the mode transducer $=70\%$ (determined from scatter parameter measurement). Then

$$G_{db}=10 \log_{10} \frac{350 \times 100 \times 100}{1000 \times 70}=16.99\ db.$$

The measured and theoretical values of gain of the aerials are tabulated in Table 4. The theoretical gain is calculated from the following relation

$$G=\frac{r^2 \mid E_p \mid^2 / 2\eta_0}{P/4\pi} \quad [11]$$

where, for

(*a*) Uniform rod

$$|E_P|=\left[E_{PS}^2+E_{P_e}^2+2 E_{PS} E_P \sin \frac{L}{2}(\beta-k \cos \theta)\right]^{1/2} \quad [12]$$

E_{PS} is given by equation [7] and

$$E_{Pe}=\left[B\frac{1}{2r}\left(\frac{\mu_0}{\epsilon_0}\right)^{1/2} a\,k\,k_1'\,J_1(k_1'\,a)\right]\times$$

$$\left[\left(k\cos\theta+\frac{\beta}{\epsilon_{r1}}\right)\frac{J_0(ka\sin\theta)\sin\theta-[k_1'\,J_0(k_1'\,a)/k\,J_1(k_1'\,a)]\,k_1\,J_1(ka\sin\theta)}{(k_1')^2-(k\sin\theta)^2}\right]$$

and the total power flow P is given by

$$P=\left[\frac{\pi\,B^2\,\beta\,a^2(k_1')^2}{2\,\omega\,\epsilon_0\,\epsilon_{r1}}\right]\left[\{J_0(k_1'\,a)\}^2+\{J_1(k_1'\,a)\}^2\right.$$

$$-\left\{\frac{2\,J_0(k_1'\,a)\,J_1(k_1'\,a)}{(k_1'\,a)}\right\}+\left\{\frac{1}{\epsilon_{r1}}\frac{k_1'^2}{k_2'}\left(\frac{J_0(k_1'\,a)}{H_0^{(1)}\,(k_2'\,a)}\right)^2\right\}\times$$

$$\left\{H_0^{(1)}\,(k_2'\,a)\right\}^2+\left\{H_1^{(1)}\,(k_2'\,a)\right\}^2-\left\{\frac{2\,H_0^{(1)}\,(k_2'\,a)\,H_1^{(1)}\,(k_2'\,a)}{k_2'\,a}\right\}$$

and

$$\eta_0=\sqrt{\left(\frac{\mu_0}{\epsilon_0}\right)} \qquad [13]$$

(*b*) Corrugated Rod.

$$|E_P|=[E_{PS}^2+E_{Pe}^2+2\,E_{PS}\,E_P\,\sin(L/2)\,(\beta-k\cos\theta)]^{1/2} \qquad [14]$$

where E_{PS} is given by equation [9] and

$$E_P=\left[\frac{C_2\,ka}{k_1}(k\,\epsilon_{r1}\cos\theta+\beta)\right]\times$$

$$\left[\frac{k_1\,J_1\,(ka\sin\theta)\,J_0(k_1\,a)-(k\sin\theta)\,J_1(k_1\,a)\,J_0(ka\sin\theta)}{k_1^2-(k\sin\theta)^2}\right]$$

$$P=\left[\frac{\pi\,\beta\,k\,A_2^2}{2\,\eta_0}\right]\left[\left\{\frac{a^2\,\epsilon_{r1}}{k_1^2}\,C_2^2\right\}\left\{[J_0(k_1\,a)]^2+[J_1(k_1\,a)]^2-\left(\frac{2\,J_0(k_1\,a)\,J_1(k_1\,a)}{k_1a}\right)\right\}\right.$$

$$+\left\{\frac{\epsilon_{r2}\,b^2}{k_2^2}\right\}\left\{[J_0(k_2\,b)]^2+[J_1(k_2\,b)]^2-\left(\frac{2\,J_0(k_1\,a)\,J_1(k_2\,b)}{k_2\,b}\right)\right\}$$

$$+\left\{b^2\,C_1^2\right\}\left\{[Y_0(k_2\,b)]^2+[Y_1(k_2\,b)]^2-\left(\frac{2\,Y_0(k_2\,b)\,Y_1(k_2\,b)}{k_2\,b}\right)\right\}$$

$$+ \{b^2 C_1\} \left(J_1(k_2 b)\, Y_1(k_2 b) - \frac{J_0(k_2 b)\, Y_1(k_2 b)}{k_2 b} \right.$$

$$\left. + J_0(k_2 b)\, Y_0(k_2 b) - \frac{Y_0(k_2 b)\, J_1(k_2 b)}{k_2 b} \right)$$

$$- \{a^2\} \left\{ [J_0(k_2 a)]^2 + [J_1(k_1 a)]^2 - \left(\frac{2\, J_0(k_2 a)\, J_1(k_2 a)}{k_2 a} \right) \right\}$$

$$- \{a^2 C_1^2\} \left\{ [Y_0(k_2 a)]^2 + [Y_1(k_2 a)]^2 - \left(\frac{2\, Y_0(k_2 a)\, Y_1(k_2 a)}{k_2 a} \right) \right\}$$

$$- \{a^2 C_1\} \left\{ J_1(k_2 a)\, Y_1(k_2 a) - \frac{J_0(k_2 a)\, Y_1(k_2 a)}{k_2 a} \right.$$

$$\left. + J_0(k_2 a)\, Y_0(k_2 a) - \frac{Y_0(k_2 a)\, J_1(k_2 a)}{k_2 a} \right\}$$

$$+ \left\{ \frac{b^2 C_3^2}{k_3^2} \right\} \left\{ [H_0^{(1)}(k_3 b)]^2 + [H_0^{(1)}(k_3 b)]^2 - \left(\frac{2\, H_0^{(1)}(k_3 b)\, H_1^{(1)}(k_3 b)}{k_2 b} \right) \right\} \Bigg| \quad [15]$$

$$C_1 = \frac{(k\, \epsilon_{r2}/k_2)\, J_1(k_2 b) - J_0(k_2 b)}{Y_0(k_2 b) - (k\, \epsilon_{r2}/k_2)\, C\, Y_1(k_2 b)}$$

$$C_2 = \frac{J_0(k_2 a) + C_1\, Y_0(k_2 a)}{J_0(k_1 a)}$$

$$C_3 = \frac{J_0(k_2 b) + C_1\, Y_0(k_2 b)}{H_0^{(1)}(k_3 b)}$$

$$C = \frac{k_3}{k}\, \frac{H_0^{(1)}(k_3 b)}{H_1^{(1)}(k_3 b)}$$

So the gain of uniform and corrugated rods are calculated from equation [11]. The measured and calculated values of gain are compared in Table 4.

9. MEASUREMENT OF E_0- MODE TRANSDUCER CHARACTERISTICS

The characteristics of mode transducer (See Fig. 26) which can be represented as a four terminal network (See Fig. 27) are measured by using Deschamp's method[3,4]. The experimental set-up for measuring the scattering parameters S_{11}, S_{12} and S_{22} is shown in Fig. 28. The circle

TABLE 4

Measured and calculated values of Gain

Structure Number	Measured value of gain (db)	Theoretical value of gain (db) (Case A) Case B	Structure Number	Measured value of gain (db)	Theoretical value of gain (db) (Case A) Case B
1u	13.22	(12.56) 13.36	5C	15.82	(15.65) 16.07
2u	12.78	(12.33) 13.36	6C	7.78	(9.44) 7.50
3u	11.76	(11.48) 12.75	7C	1.76	([illegible].96) 1.66
4u	10.79	(11.28) 11.96	8C	3.01	(1.77) 2.30
5u	12.80	(12.68) 13.55	9C	4.91	(4.51) 4.41
6u	11.14	(10.78) 12.03	10C	16.99	(17.97) 17.99
7u	10.05	(10.27) 11.53	11C	12.79	(12.25) 12.44
8u	11.0	(8.81) 11.44	12C	13.22	(14.52) 14.83
9u	6.99	(3.05) 7.74	13C	14.77	(16.11) 16.15
1C	10.79	(11.40) 10.99	14C	15.84	(15.65) 15.73
2C	16.02	(16,65) 16.74	15C	7.02	(6.73) 6.96
3C	16.02	(16.85) 17.13	16C	15.55	(16.53) 16.60
4C	15.44	(16.29) 16 28			

diagram (See Fig. 29) using appropriate experimental data is drawn (See Appendix A.3). The scattering coefficients (See Appendix A.4) are evaluated.

$$S_{11}=0.16 \ \exp\ (j\, 5.9 \text{ rad})$$
$$S_{12}=0.855 \ \exp\ (j\, 0.087 \text{ rad}) \qquad [16]$$
$$S_{22}=0.197 \ \exp\ (j\, 3.2 \text{ rad})$$

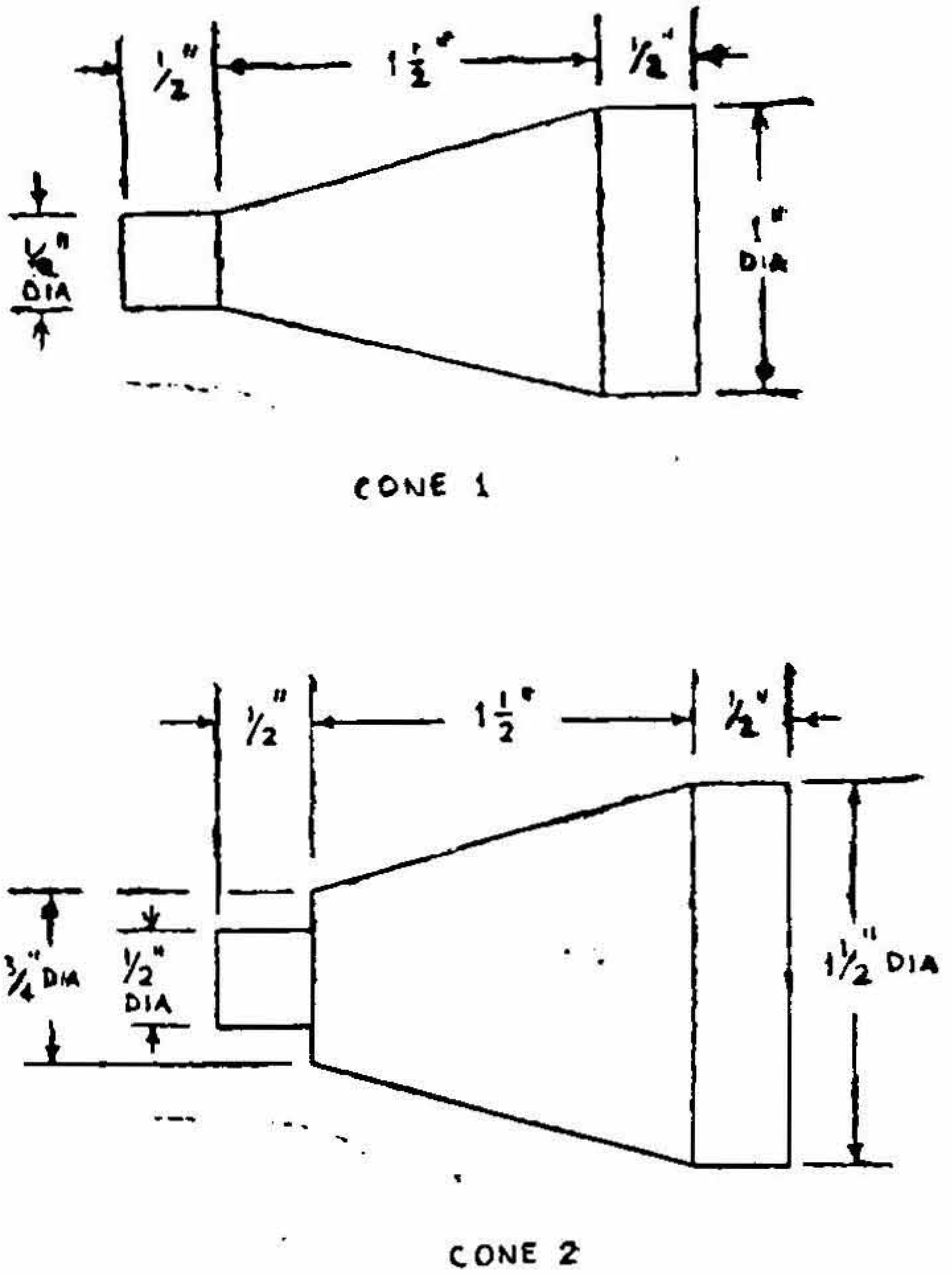

FIG. 26

Dimensional sketches of the launching cones.
wall thickness $\frac{1}{16}$" Material : Brass

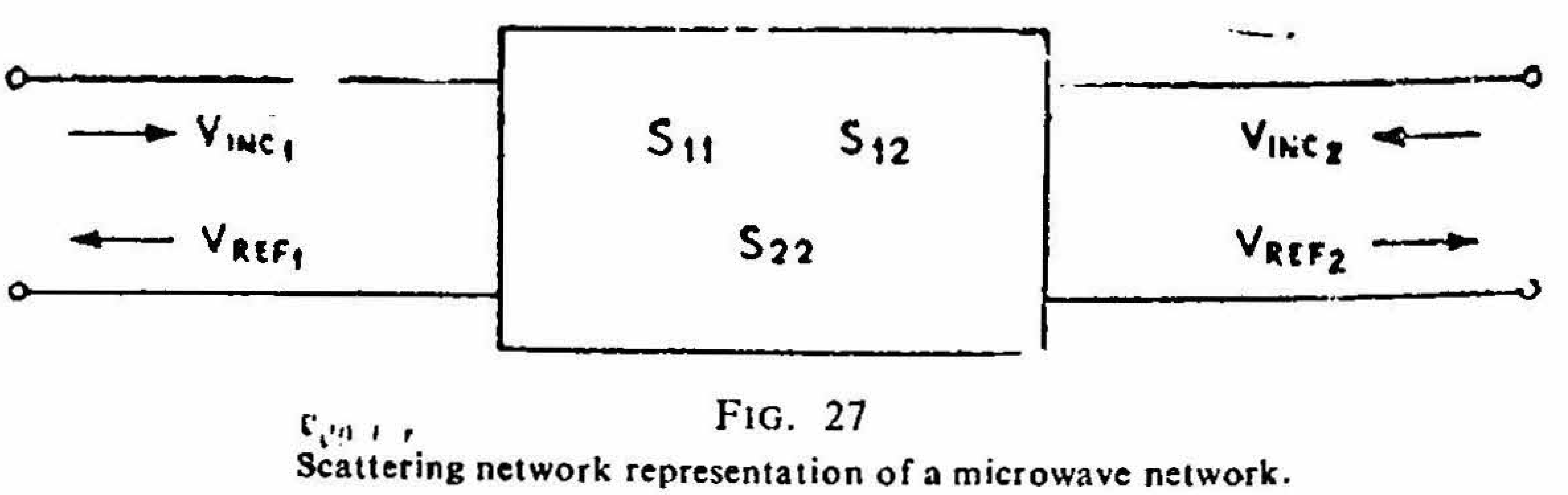

FIG. 27

Scattering network representation of a microwave network.

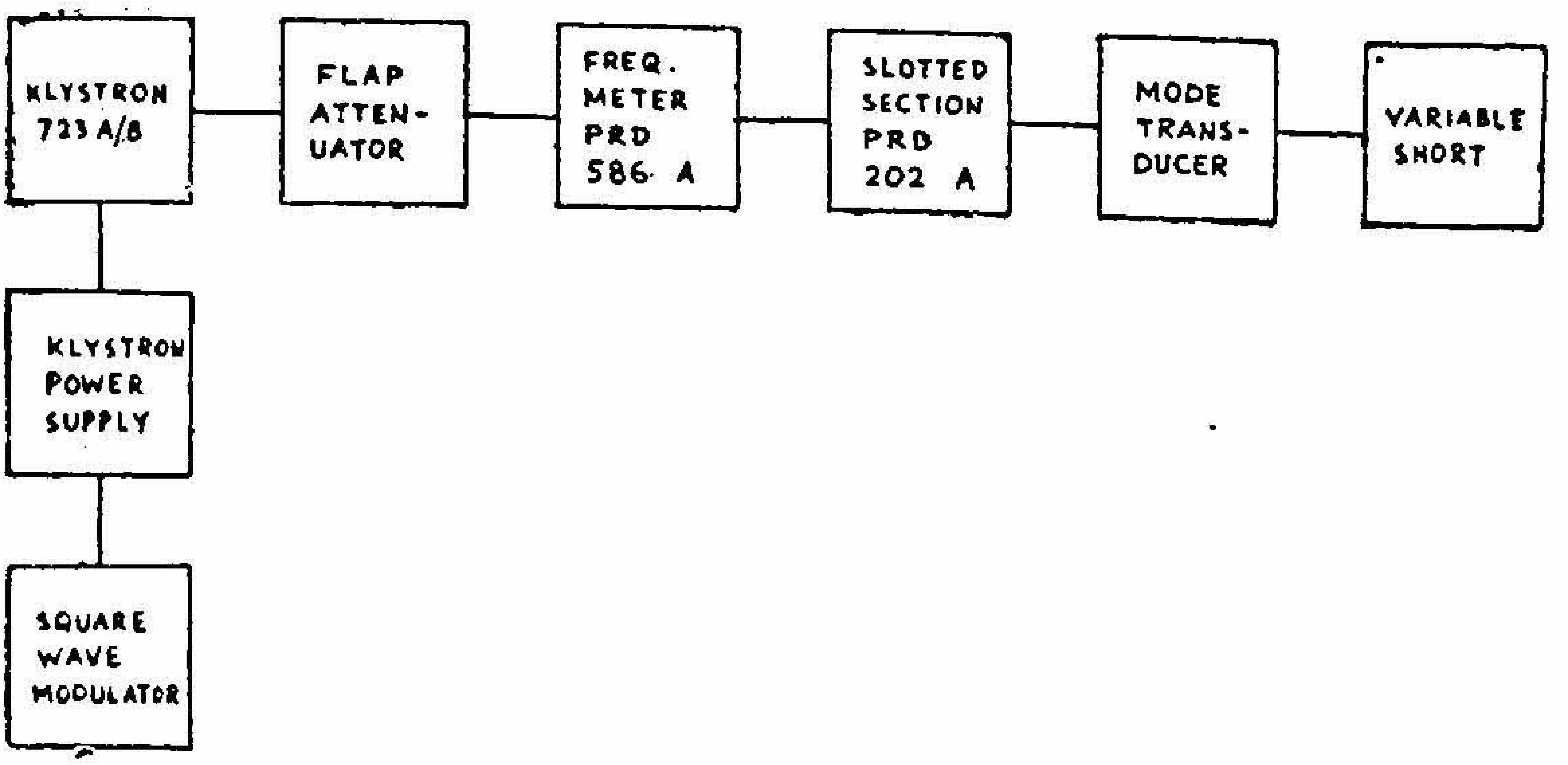

FIG. 28

Experimental set up for measurement of scattering matrix of mode transduces.

9.1 *Insertion Loss* (L).

The insertion loss (L) of the mode transducer is given by,

$$L\ (db) = -10 \log_{10} (1 - |S_{11}|^2) - 10 \log_{10} \frac{|S_{12}|^2}{1 - |S_{11}|^2} = 1.56\ db. \qquad [17]$$

9.2 *Reflection Loss* (L_R)

The reflection loss at the input terminals of the mode transducer is

$$L_R\ (db) = -10 \log_{10} (1 - |S_{11}|)^2 = 0\ 086\ db \qquad [18]$$

9.3 *Dissipation Loss* (L_D).

The dissipation loss in the network is given by

$$L_R(db) = -10 \log_{10} \frac{|S_{12}|^2}{1 - |S_{11}|^2} = 1.474\ db. \qquad [19]$$

9.4 *Transmission Efficiency* η_t.

The transmission efficiency of the mode transducer is

$$\eta_t = \frac{|S_{12}|^2}{1 - |S_{11}|^2} = 75.02\% \qquad [20]$$

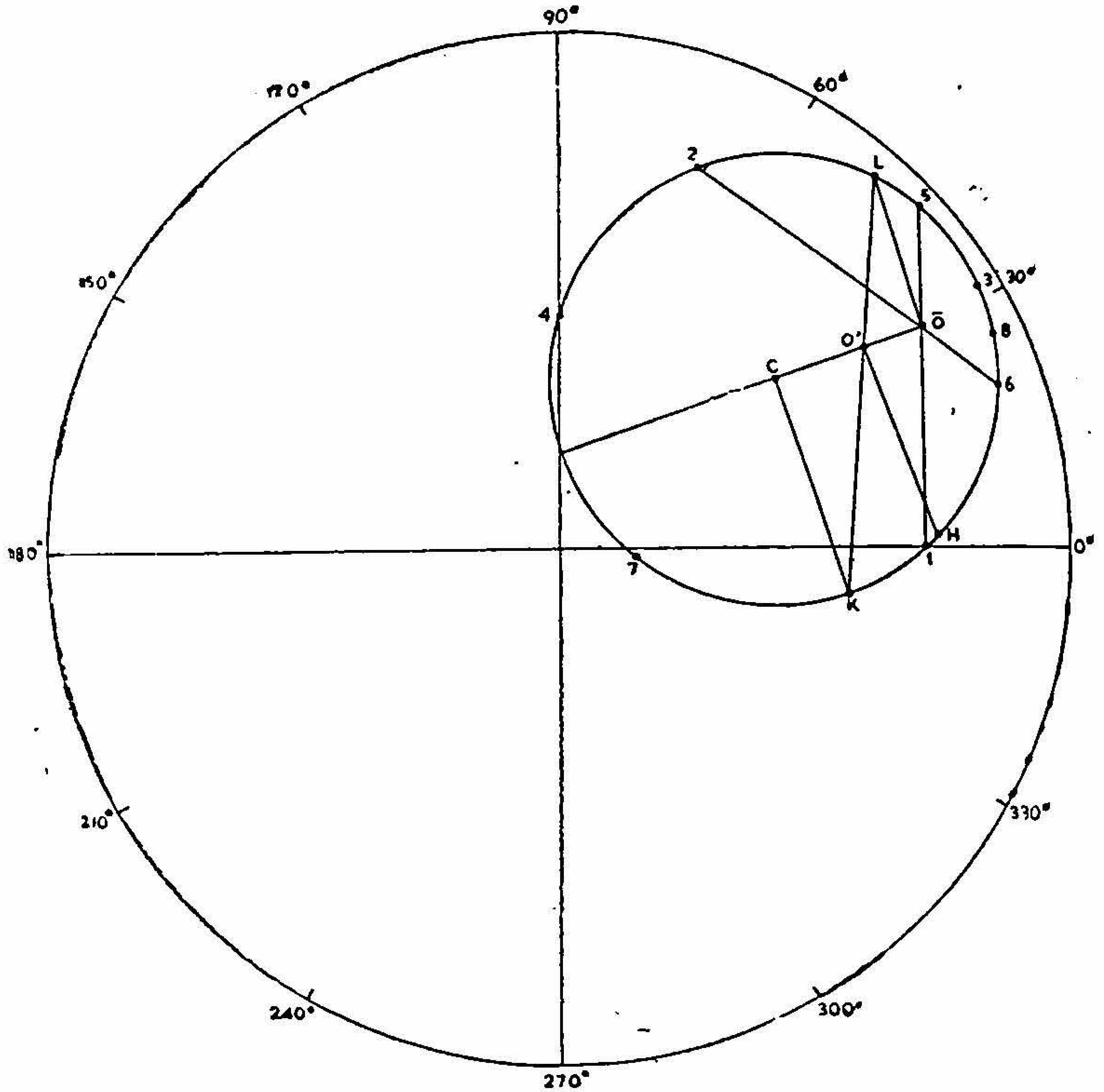

FIG. 29

Circle diagram leading to the evaluation of scattering mattrix (*S*).

9.5 *Launching Efficiency of the Mode Transducer* η_L.

The launching efficiency of the mode transducer is given by (See Appendix A.5)

$$\eta_L = \frac{1-|\sigma_{11}|^2}{|1-\sigma_{11}S_{22}|^2}|S_{12}|^2 \tag{21}$$

where, σ – is the scattering matrix of the dielectric rod which is fitted to the mode transducer.

The σ – matrix is determined by the method described elsewhere[4]. From the v.s.w.r. and positions of minimum for different lengths of the rod a second circle diagram is drawn (See Fig. 30). The scattering coefficient Σ of the combined network consisting of the mode transducer and the dielectric rod is determined from the circle diagram. The scattering coefficient Σ_{11} is given by

$$\Sigma_{11} = 0.18 \exp j\ (3.48 \text{ rad}) \tag{22}$$

The scattering coefficient σ_{11} of only the dielectric rod is obtained by S – matrix and Σ – matrix by the following relation (See Appendix A.3)

$$\Sigma_{11} = S_{11} + \left(\frac{S^2{}_{12}}{1-\sigma_{11}S_{22}}\right)\sigma_{11} \tag{23}$$

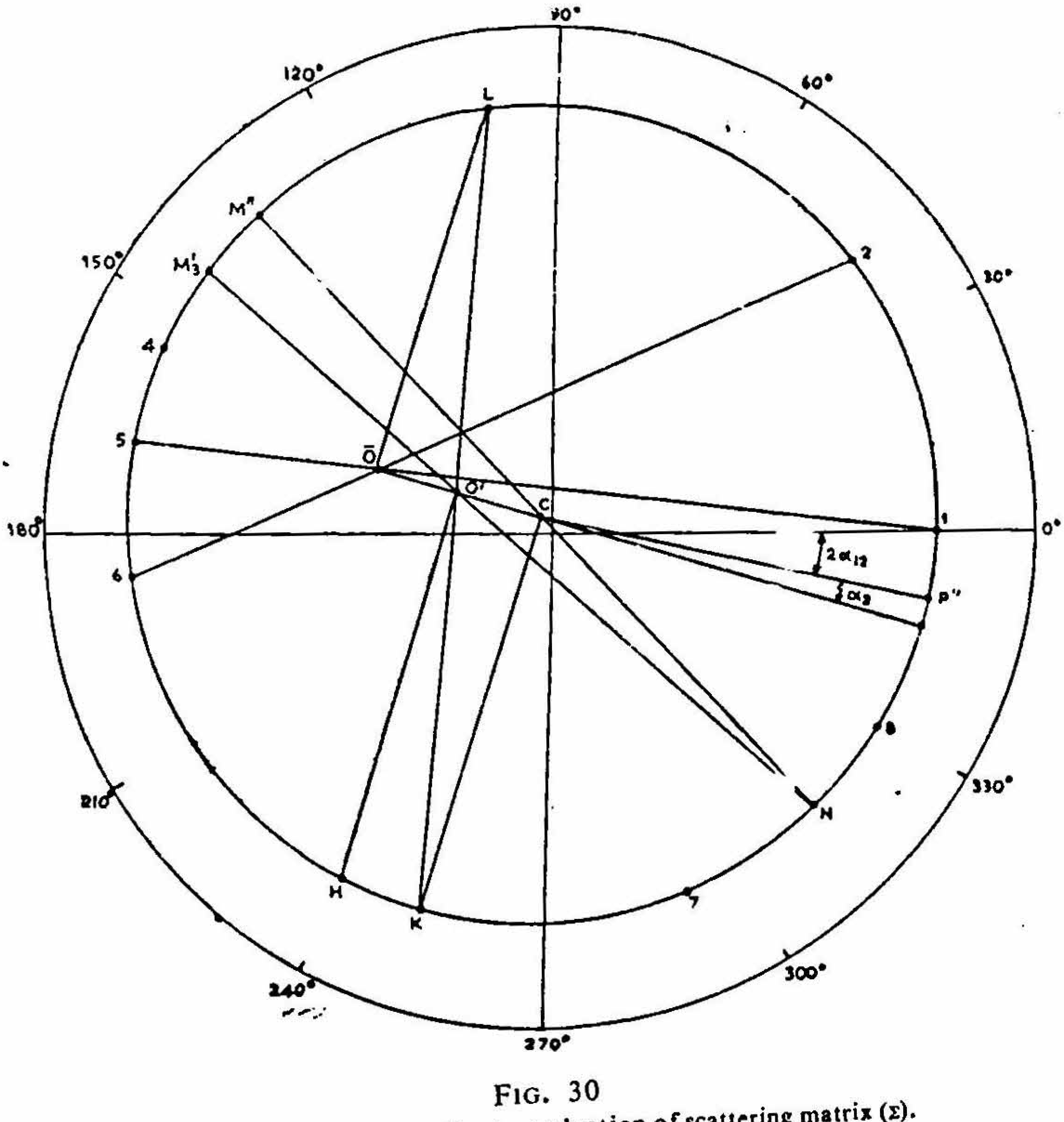

FIG. 30

Circle diagram leading to evaluation of scattering matrix (Σ).

Substituting the values of S_{11} and Σ_{11} from equations (16-22), the value of the scattering coefficient for the dielectric rod is

$$\sigma_{11} = 0.4026 \exp j\ (0.1218 \text{ rad}) \qquad [24]$$

The launching efficiency is

$$L = 73.96\ \%.$$

10. DISCUSSION.

10.1 *Purity of the Surface Wave Mode.*

The agreement between theoretical and experimental values of decay coefficient (ξ), guide wavelength, gain and radiation characteristics shows that the surface wave mode E_0 launched on the corrugated structure is practically free from contamination of other modes. It also shows that the assumption of treating the corrugated guide as a homogeneous structure of effective dieletric constant

$$\epsilon_{r2} = \left[\frac{\sqrt{\epsilon_{r1}} \cdot t + s}{t + s} \right]^2 \qquad [25]$$

is justified.

10.2 *Cut-off-Conditions.*

The cut-off condition is significantly influenced by corrugation. For example, a uniform dielectric rod $\epsilon_r = 2.56$ excited in E_0-mode at $\lambda_0 = 3.14$ cm has a cut-off radius = 0.9624 cm., whereas, a corrugated rod of inner dielectric rod radius, $a = 0.2$ cms, disc radius $b = 2.54$ cm, disc spacing, = $s = 0.5$ cm. and disc thickness, $t = 0.3175$ cm can support a pure surface wave E_0-mode.

10.3 *Surface-wave Field and Radiated wave field.*

The correlation of the radiated wave field and near field (See Fig. 31-33) show that

(i) The position of major lobe for a particular value of $\lambda g/\lambda_0$ (for different structures) remains the same within $\pm 2°$ (See Fig 31).

(ii) The 3-*db* beam width of the major lobe for a particular value of $\lambda g/\lambda_0$ (of different structures) remains the same within $\pm 2°$ (See Fig. 32).

(iii) The number of lobes (maxima) for a particular value of $\lambda g/\lambda_0$ which are above -20 *db* differ significantly in different cases. Also, the number of lobes in cases A and B are different (See Fig. 33).

The variation of gain with $\lambda g/\lambda_0$ is shown in Fig. 34.

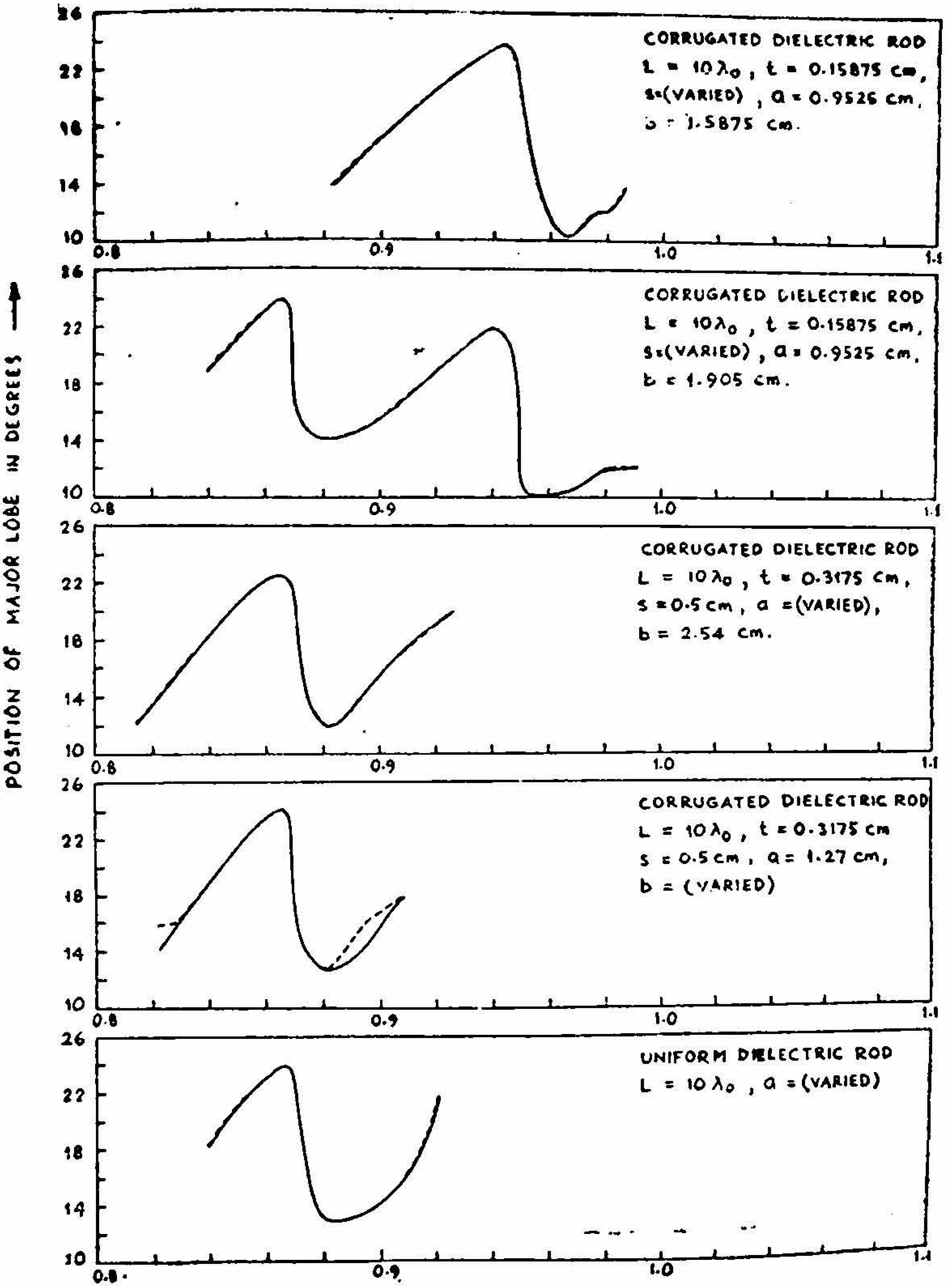

FIG. 31

Position of major lobe *vs* $\lambda g/\lambda_0$.

t=Disc thickness, *s*=Disc spacing, *a*=Inner rod radius, *b*=Disc radius.

—Case *A* Case *B*.

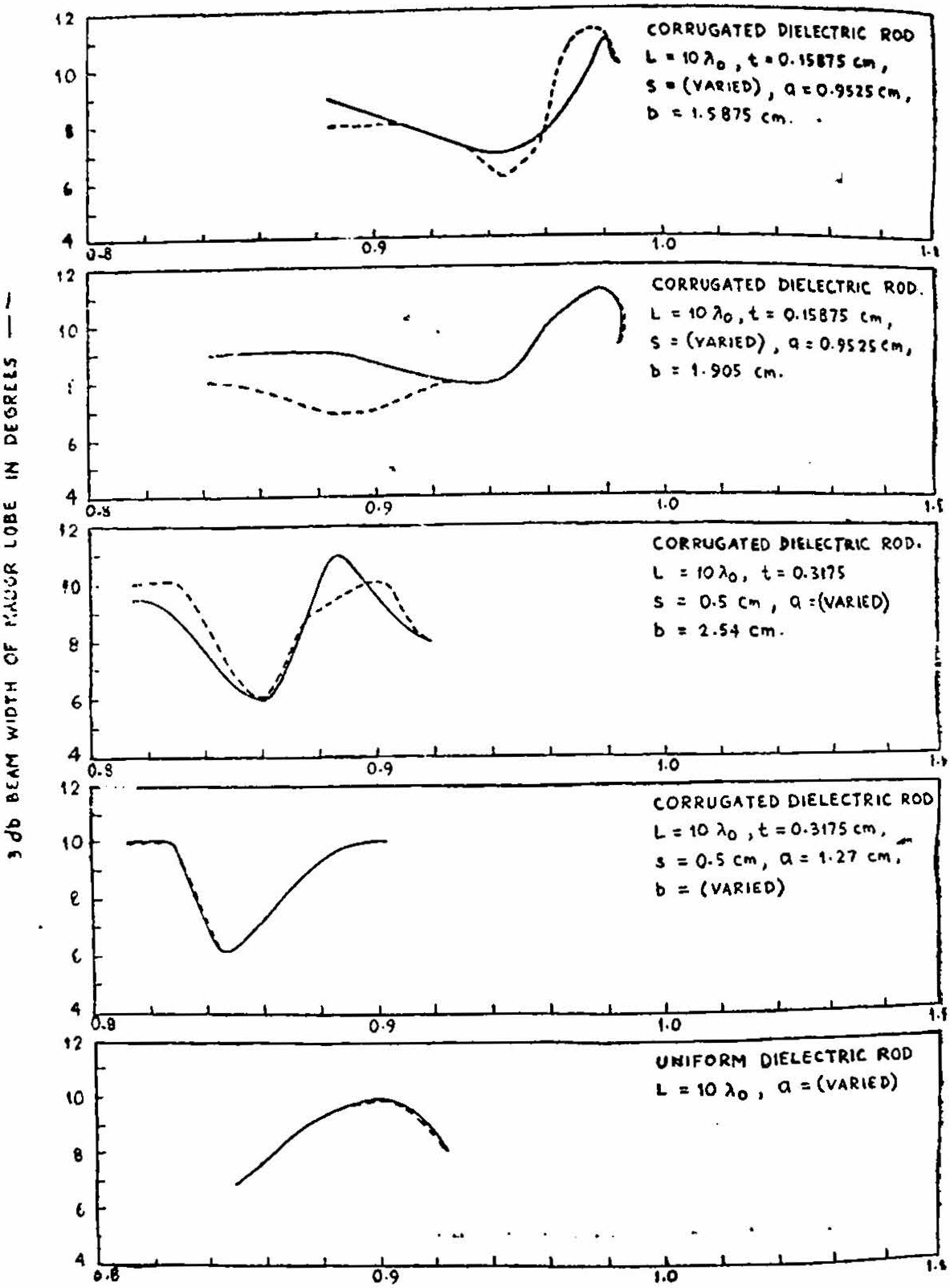

FIG. 32

3*db* Beam width of major lobe *vs.* $\lambda g/\lambda_0$.

t=Disc thickness, *s*=Disc spacing, *a*=Inner rod radius, *b*=Disc radius.

—Case *A* Case *B*

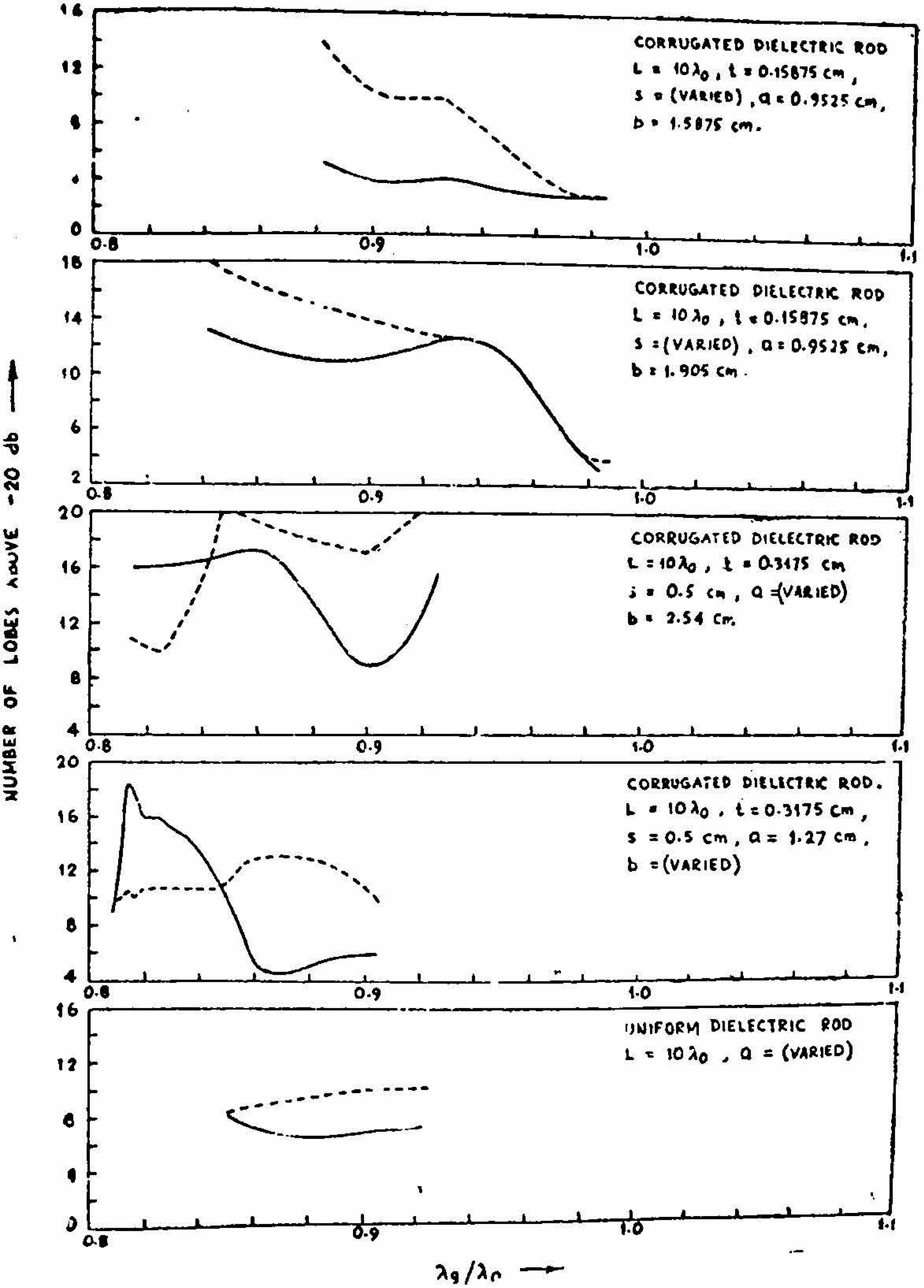

FIG. 33

Number of lobes *vs* $\lambda g/\lambda_0$.

. = Disc thickness, *s* = Disc spacing, *a* = Inner rod radius, *b* = Disc radius.

— Case *A* Case *B*

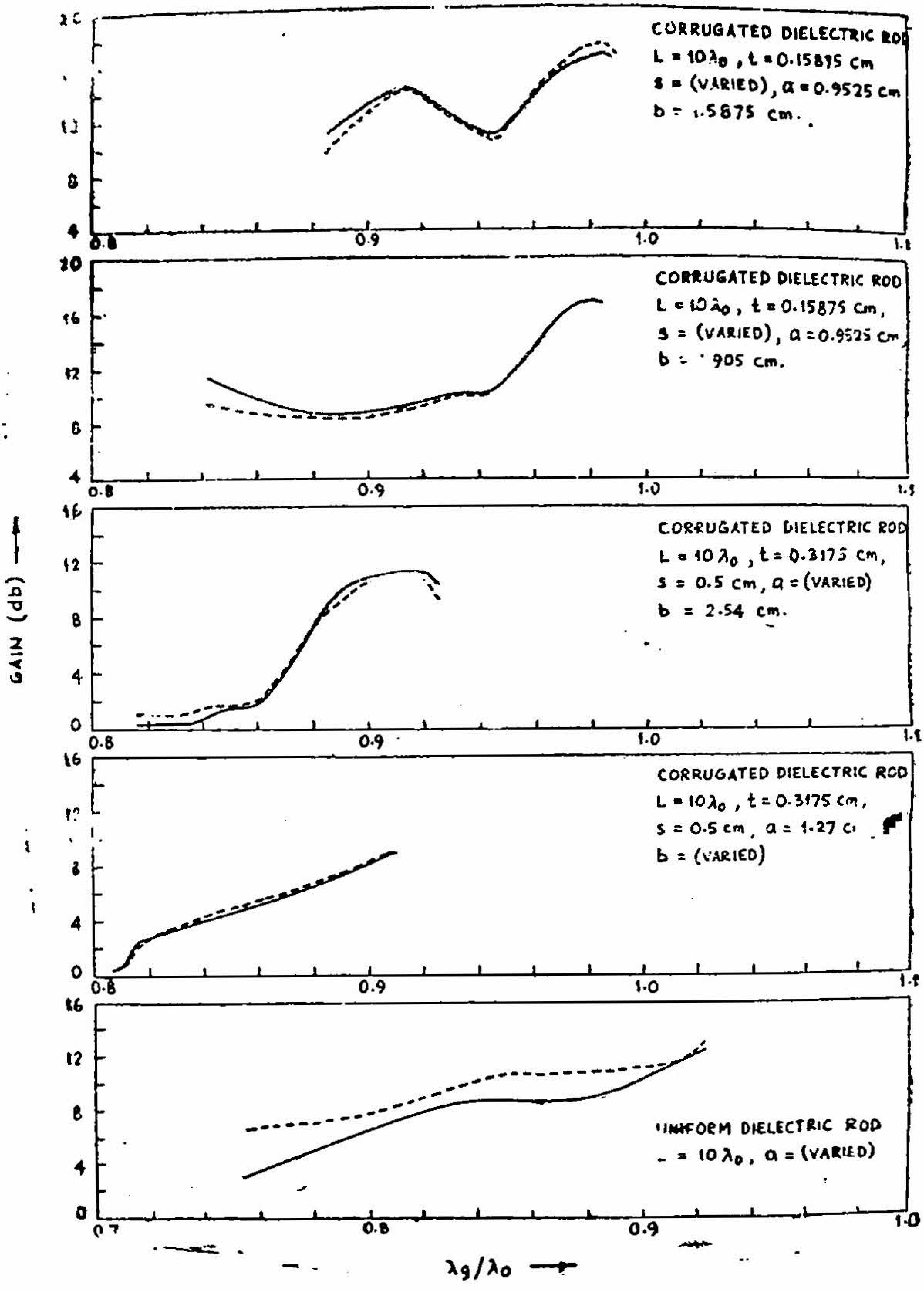

FIG. 34

Variation of gain with $\lambda g/\lambda_0$.

t — Disc thickness, s — Disc spacing, a — Inner rod radius, b — Disc radius.

— Case A — Case B

10.4 *Comparison of Uniform and Corrugated Dielectric Rods Characteristics.*

The corrugated rod can be cosidered as a uniform dielectric rod of radius '*a*' loaded with dielectric dics of radius '*b*' or it can be considered as a grooved uniform rod of radius '*b*'. It may therefore, be worthwhile to compare the performance of the corrugated dielectric rod with uniform dielectric rod of radius '*a*' and '*b*'. The characteristics such as decay coefficients, attenuation constants, gain, etc of the uniform and corrugated rods are compared in tables 5-9.

11. CONCLUSIONS

(i) The corrugated rod can act as a better surface wave guide than a uniform rod.

(ii) The corrugated rod can support surface wave of longer wavelength than uniform rod when excited in E_0 – mode.

(iii) The radiation characteristics of a corrugated rod can be controlled by adjusting groove depth and spacing.

(iv) The corrugated rod shows better radition characteristics with regard to number and relative intensity of minor lobes and gain compared to uniform dielectric rod.

(v) It is possible to predict the nature of the far field from a measurement of the surface wave field.

TABLE 5

Decay Coefficients ξ of uniform and corrugated Dielectric Rod

Structure Parameters				$\xi = k_s$ (cm^{-1})	ξcm^{-1} of rod of radius '*a*'	ξ(cm^{-1}) of rod of radius '*b*'	Radius of uniform rod which gives $\xi = k_s$
t(cm)	*s*(cm)	*a*(cm)	*b*(cm)				
0.3175	0.5	1.27	1.4288	1 035	0.826	1.22	1.35
0.1588	0.5	1.27	1 508	1.027	0 826	1.30	1.32
0.3175	0.5	1 27	2.54	1.4065	0.826	2.067	1.58
0.3175	0.3	1.27	2.54	1.5472	0.826	2.067	1.75
0.3175	0 5	1.27	2.0	1.3151	0.826	1.84	1.50
0.3175	0.5	1.27	3.0	1.44	0.826	2.20	1.62
0.1588	0.5	1.27	1.7	1.10	0.826	1.52	1.42
0.3175	0.5	0.6	2.54	0.9346	cut-off	2.067	1.28
0.1588	1.0	2.225	2.858	0.3999	1.938	2.159	cut-off
0.1588	1.6	2.25	3.175	0.3823	1.938	2.222	cut-off

TABLE 6

Attenuation constant of corrugated (α) and uniform (α) of dielectric rods

Structure Parameters				α(db/m) measured	α(db/m) rod radius 'a' cm (measured) calculated	α(db/m) rod radius 'b' cm (measured) calculated
t(cm)	s(cm)	a(cm)	b(cm)			
0.1588	0.4	0.9525	1.5875	3.92	cut-off	(6.53) 6.4
0.1588	1	0.9525	1.5875	4.20	cut-off	(6.53) 6.4
0.3175	0.5	0.8	2.54	3.63	cut-off	(7.5)
0.1588	0.5	1.27	2.54	4.01	(4.53) 4.25	(7.5)
0.1588	0.5	1·27	1.4288	4.3	(4.55) 4.25	(5.20) 5.255
0.1588	1	0.9525	1.27	3.2	cut-off	(4.55) 4.25
0.1588	1	2.2225	2.8575	4.67	7.23	(7.67)
0.1588	1	0.9525	1.905	4.31	cut-off	(6.97) 7.15
0.1588	1.6	2.2225	3.175	4.44	(7.23)	(7.83)
0.1588	1	0.9525	2.2225	4.35	cut-off	(7.23)

The theoretical α-values of uniform rods are calculated using Elasser's[5] results (See Appendix A.6).

Table 7

Radiation Characteristics (Case A)

Corrugated Dielectric Rod							Uniform rod of radius 'a' cm.			Uniform Rod of radius 'b' cm.		
Structure Parameters				Angular position and intensity of minor lobe of highest level	3 *db* Beam width of major lobe	Total Number of lobes above —20 *db*	Angular position and intensity of minor lobe of highest intensity	3 *db* Beam width of major lobe	Total Number of lobes above —20 *db*.	Angular position and intensity of minor lobe of highest level	3 *db* Beam width of major lobe	Total number of lobes above —20 *db*.
t(cm)	s(cm)	a(cm)	b(cm)									
0.1588	1.4	.9525	1.5875	30° (0.121) −9.16*db*.	10°	3	—	—	—	34° (.51) −2.87*db*.	7°	8
0.1588	1.3	0.9525	1.905	28° (0.117) −9.29*db*.	11°	4	—	—	—	28° (.867) −.61*db*.	9°	14°
0.3175	0.5	1.27	1.4288	28° (.83) −0.66*db*.	11°	5	34° (.47) −3.27*db*.	8°	7	28° (.79) −.98*db*.	10°	7°
0.1588	0.5	1.27	1.508	28° (0.72) −1.39*ab*.	10°	5	34° (0.47) −3.27*db*.	8°	7	36° (.45) −3.425*dq*	9°	7°
0.3175	0.5	1.905	2.54	42° (0.031) −15.01 *db*.	10°	4	28° (0.867) −0.61*db*.	9°	14	26° (.65) −1.88*db*.	8°	18°
0.1588	1	2.2225	2.8575	40° (0.037) −14.37*db*.	10°	4	32° (0.349) −4.56*db*.	8°	18	8° (0.26) −5.8*db*.	7°	18

TABLE 8

Radiation Characteristics (Case B)

Structure Parameters				Corrugated Rod			Uniform Rod Radius 'a' cm.			Uniform dielectric Rod of radius 'b'		
t(cm)	*s*(cm)	*a*(cm)	*b*(cm)	Angular position and intensity of minor lobe of highest intensity	3 *db* Beam width of major lobe	Total Number of lobes above −20 *db*	Angular position and intensity of minor lobe of highest intensity	3 *db* Beam width of major lobes	Total number of lobes above −20 *db*	Angular position and intensity of minor lobe of highest intensity	3 *db* Beam width of major lobe	Total number of lobes above −20 *db*.
.1588	1.4	.9525	.5875	30° (.132) −8.79*db*.	10°	3	–	–	–	34° (.728) −1.376*db*.	7°	10
.1588	1.3	.9525	1.905	28° (.12) −9.17*db*.	11°	4	–	–	–	28° (.89) −.5*db*.	9°	13
.3175	0.5	1.27	1.4288	28° (.87) −.58*db*.	11°	12	34° (.577) −2.38*db*	8°	10	28° (.98) −.069*db*.	10°	10
.1588	0.5	1.27	1.508	28° (.808) −.92*db*.	10°	10	34° (.571) −2.38*db*.	8°	10	36° (.634) −1.97*db*.	9°	9
.3175	0.5	1.905	2.54	42° (.042) −13.76*db*.	10°	6	28° (.89) −.5*db*,	9°	13	26° (.7) −1.55*db*.	8°	13
.1588	1	2.2225	2.8575	40° (.045) −13.4*db*.	10°	4	32° (.86) −.64*db*	9°	11	32° (.65) −1.86*db*.	7°	7

TABLE 9

Comparison of Gain

Corrugated Dielectric Rod					Uniform Rod of radius '*a*' cm.	Uniform Rod of radius '*b*' cm.
Structure Parameters (cm)				Gain (*db*) (Case A) Case B	Gain (*db*) (Case A) Case A	Gain (*db*) (Case A) Case B
t	*s*	*a*	*b*			
0.1588	1.0	0 9525	1 27	(17.97)	--	(12.33)
				17.99	–	13.29
0.1588	1.2	.9525	1.5875	(16.82)	–	(8.808)
				17.00	–	11.44
0.1588	1.6	.9525	1.905	(16.25)	–	(3.051)
				16.33	–	7.736
0.3175	0.5	1.905	2.54	(6.55)	(3.051)	Very small
				6.45	7.736	6.5
0.1588	1.0	2.2225	2.8575	(17.24)	(1.415)	Very small
				17.35	7.0	6.0
0.1518	1.0	0.9525	1.4288	(12.25)	–	10.27
				12.44	–	11.53
0.1588	1.6	2.2225	3.175	(16.54)	1.415	Very small
				16.6	7.0	5.5
0.3175	0.5	0.6	2.54	(11.78)	–	Very small
				11.78	–	6·0

12. APPENDIX

A.1 *Specifications of uniform dielectric rods used for experiment* :

L = length of rod (cms)

a = radius of rod (cms)

$\lambda_0 = 3.14$ cms.

Structure Number	L/λ_0	a/λ_0	Remarks
1 u	12	0.4045	*
2 u	10	0.4045	*
3 u	8	0.4045	*
4 u	6	0.4045	*
5 u	4	0.4045	*
6 u	2	0.4045	
7 u	10	0.455	
8 u	10	0.505	
9 u	10	0.606	
10 u	10	0.708	
11 u	10	0.808	**
12 u	10	0.91	**

*Not used for surface wave field measurement.
**Not used for radiation field measurement.

A.2 *Specifications of corrugated dielectric rod*.

$L = 31.4$ cm $= 10$ (cm)
$t =$ thicness of discs (cm)
$s =$ spacing of discs (cm)
$a =$ radius of inner rod (cm)
$b =$ radius of discs (cm)
$\lambda_0 = 3.14$ cm, $(1/16)'' = 0.15875$ cm, $(1/8)'' = 0.3175$

Structure Number	t (cms)	s/λ_0	a/λ_0	b/λ_0
1 C	.15875	.1273	.303	.505
2 C	.15875	.3184	.303	.505
3 C	.15875	.414	.303	.505
4 C	.15875	.5095	.303	.505
5 C	.15875	.6369	.303	.505
6 C	.3175	1592	.2546	.8089
7 C	.3174	.1592	.3184	.8089
8 C	.3175	.1592	.4045	.8089
9 C	.3175	.1592	.6066	.8089
10 C	.15875	.3184	.303	.4045
11 C	.15875	.3184	.303	.455
12 C	.15875	.3184	.303	.6066
13 C	.15875	.3184	.303	.7085
14 C	.15875	.3184	.3184	.4045
15 C	.15875	.1592	.4045	.455
16 C	.15875	.5095	.7085	1.011
17 C	.15875	.1592	.2546	.4045
18 C	.15875	.3184	.2022	.4045
19 C	.15875	.6369	.1011	.4045

A.3 *Construction of circle diagram.*

The procedure for constructing the circle diagram is as follows (See Fig 29).

(i) The position of the variable short is varied by equally spaced smalle intervals ($\lambda g/16$) and at each setting the position of the first minima D_j and the voltage standing wave ratio are noted. The observations are numbered 1, 2, 3, · · · 8. The reflection coefficient is calculated in each case by using the following relations

$$\left| \Gamma_j \right| = \frac{\gamma_j - 1}{\gamma_j + 1}$$

and $\theta_j = 4\pi\, d_j/\lambda g$. where. d_j represents the shift in the first voltage minima from the reference plane.

(ii) The rflection coefficients obtained are plotted. The circle accommodating the plotted points is drawn with C as centre.

(iii) The points 1 and 5, 2 and 6, · · · · · · are joined, the point of intersection of these lines **0** is noted.

(iv) The iconocentre 0′ is then determined in the following manner. The points C and **0** aae joined by a straight line A line perpendicular to C **0** through **0** is drawn to intersect the locus at L and another through C perpendicular to C **0** to intersect the at K. The points L and K are joined and the point of intersection of L K with C **0** is 0′ the iconocentre. $C0'$ in polar coordinates gives the magnitude of S_{11}. The angle θ' of the point 0′ is noted. Then

$$S_{11} = \left| C\ 0' \right| j(\theta' \pm \pi)$$

and $S_{22} = C\ 0'/R$ where, R is the radius of the locus.

(v) The magnitude of S_{12} is obtained by drawing a line through 0′ perpundicular to C 0 to intersect the circle at H. Then

$$S_{12} = 0'H/\sqrt{R}$$

(vi) For any particular setting of the variable short, the angle $\theta_s = 4\pi d_s/\lambda g$ is computed. The data point corresponding to S is marked as M' and a line is drawn M' through O' to intersect the locus at N. From N through C, a line is drawn to intersect the locus at M''.

(vii) About C as centre, an angle $\phi = 360^0 - \theta_s$ from the line $C\ M''$ is marked in the counter-clockwise direction. At that angle a line through C is drawn to intersect the circle at P''. The line 0′ C is extended.

(viii) The angle α_2 between the line $0'C$ and CP'' is noted. The angle between the positive real axis and that line $C\ P''$ gives $2\alpha_{12}$. All the angles are measnred in the counter-clockwise direction.

(ix) The phases of S_{22} and S_{12} are as follows

$$\arg S_{22} = \alpha_2 \pm \pi$$

$$\arg S_{12} = \alpha_{12}$$

A.4 *Scattering Matrix of Dielectric Rod: Cascading of S and σ Networks.*

The scattering matrix Σ refers to the whole system comprising the mode transducer and the dielectric rod. The scattering matrix of the dielectric rod is determined from the composite matrix as follows. The mode transducer and the dielectric rod are represented by 1-2 and 3-4 respectivly (See Fig. A. 4.1).

Let $\begin{pmatrix} S_{11} & S_{12} \\ S_{21} & S_{22} \end{pmatrix}$ be the scattering matrix of the mode transducer and $\begin{pmatrix} \sigma_{11} & \sigma_{12} \\ \sigma_{21} & \sigma_{22} \end{pmatrix}$ represent the scattering matrix of the dielectric rod. Then

$$\begin{pmatrix} E_{r1} \\ E_{r2} \end{pmatrix} = \begin{pmatrix} S_{11} & S_{12} \\ S_{21} & S_{22} \end{pmatrix} \begin{pmatrix} E_1 \\ E_2 \end{pmatrix} \tag{A.4.1}$$

and

$$\begin{pmatrix} E_{r3} \\ E_{r4} \end{pmatrix} = \begin{pmatrix} \sigma_{11} & \sigma_{12} \\ \sigma_{21} & \sigma_{22} \end{pmatrix} \begin{pmatrix} E_3 \\ E_4 \end{pmatrix} \tag{A.4.2}$$

which yield

$$E_{r1} = S_{11} E_1 + S_{12} E_2 \tag{A.4.3}$$

$$E_{r2} = S_{21} E_1 + S_{22} E_2 \tag{A.4.4}$$

$$E_{r3} = \sigma_{11} E_3 + \sigma_{12} E_4 \tag{A.4.5}$$

$$E_{r4} = \sigma_{21} E_3 + \sigma_{22} E_4 \tag{A.4.6}$$

When the two networks (See Fig. A.4.2), S and σ – are connected so that the terminals 2-2 and 3-3 are joined together

$$E_{r2} = E_3 \text{ and } E_2 = E_{r3} \tag{A.4.7}$$

Substituting (A.4 7) in (A.4.2)

$$\begin{pmatrix} E_2 \\ E_{r4} \end{pmatrix} = \begin{pmatrix} \sigma_{11} & \sigma_{12} \\ \sigma_{21} & \sigma_{22} \end{pmatrix} \begin{pmatrix} E_{r2} \\ E_4 \end{pmatrix} \tag{A.4.8}$$

Equations (A.4 5) and (A.4.6) can be written as

$$E_2 = \sigma_{11} E_{r2} + \sigma_{12} E_4 \tag{A.4.9}$$

$$E_{r4} = \sigma_{21} E_{r2} + \sigma_{22} E_4 \tag{A.4.10}$$

Eliminating E_{r2} from (A.4.9) and (A.4 4)

$$E_2 = \frac{\sigma_{11} S_{12} E_1 + \sigma_{12} E_4}{1 - \sigma_{11} S_{22}} \tag{A.4.11}$$

Substituting (A.4.11) in (A.4.3)

$$E_{r1} = \left[S_{11} + \left(\frac{S_{12}^2}{1 - \sigma_{11} S_{22}} \right) \sigma_{11} \right] E_1 + \left[S_{12} \left(\frac{\sigma_{12}}{1 - \sigma_{11} S_{22}} \right) \right] E_4 \tag{A.4.12}$$

Eliminating E_2 from (A.4 9) and (A.4.4)

$$E_{r2} = \frac{S_{12} E_1 + \sigma_{12} S_{22} E_4}{1 - \sigma_{11} S_{22}} \tag{A.4.13}$$

Substituting (A.4.13) in (A.4 6)

$$E_{r4} = \left[S_{12} \left(\frac{12}{1 - \sigma_{11} S_{22}} \right) E_1 \right] + \left[\sigma_{22} \left(\frac{\sigma_{12}}{1 - \sigma_{11} S_{22}} \right) S_{22} \right] E_4 \tag{A.4.14}$$

From Equations (A.4.12) and (A.4.14)

$$\begin{pmatrix} E_{r1} \\ E_{r4} \end{pmatrix} = \begin{pmatrix} \Sigma_{11} & \Sigma_{12} \\ \Sigma_{21} & \Sigma_{22} \end{pmatrix} \begin{pmatrix} E_1 \\ E_4 \end{pmatrix} \tag{A.4.15}$$

where, $\begin{pmatrix} \Sigma_{11} & \Sigma_{12} \\ \Sigma_{21} & \Sigma_{22} \end{pmatrix}$ is the compositre matrix of the mode transducer and the dielectric rod. The coefficient Σ_{11} is given by

$$\Sigma_{11} = S_{11} + \left(\frac{S^2{}_{12}}{1 - \sigma_{11} S_{22}} \right) \sigma_{11} \tag{A 4,16}$$

A.5 *Launching Efficiency.*

An expression for the launching efficiency of the E_0-mode transducer is obtained as follows. Assume matched load at the terminal 4-4 (See Fig. A.4.1)

$$E_4 = 0 \tag{A.5.1}$$

Snbstituting (A.5.1) in (A.4.5) and (A.4.6)

$$E_{r3} = \sigma_{11} E_3 \tag{A.5.2}$$

$$E_{r4} = \sigma_{21} E_3 \tag{A.5.3}$$

Since S and σ networks are cascaded

$$E_{r2} = E_3 \tag{A.5.4}$$

$$E_2 = E_{r3} \tag{A.5.5}$$

From Equations (A.5.2) and (A.5.5)

$$E_2 = \sigma_{11} E_3 = \sigma_{11} E_{r2} \tag{A.5.6}$$

From equations (A.5.6 and (A. .4)

$$E_{r2} = S_{21}\ E_1 + \sigma_{11}\ S_{22}\ E_{r2} \tag{A.5.7}$$

$$= (S_{21}/1 - \sigma_{11}\ S_{22})\ E_1 \tag{A.5.8}$$

Power entering the σ – network

$$P_{\sigma 1} = E_r{}^2{}_2(1 - |\sigma_{11}|^2)$$

$$\text{or, } P_{\sigma 1} = \frac{S_{12}{}^2}{|1 - \sigma_{11} S_{22}|^2}(1 - \sigma_{11}{}^2)|E_1|^2 \tag{A.5.9}$$

The launching efficiency is defined as the ratio of the power entering σ—network to the power incident on the S – network.

$$\frac{P\sigma_1}{P_{s1}} = \frac{1 - |\sigma_{11}|^2}{|1 - \sigma_{11} S_{22}|^2}|S_{22}|^2 \tag{A.5.10}$$

A.6 *Abstract from Elasser's paper* (5).

The attenuation of dielectric rod is calculated using perturbation method and the relation is

$$\alpha = 2729\ (\epsilon_r \phi/\lambda_0)\ Q\ dh/\text{meter}$$

where,

$\phi = \sigma / \omega \epsilon_1$

σ = Conductivity of the medium

Q = a dimensionless quantity

ϵ_r = relative permittivity of the rod.

The following table gives Q as a function of radius of the rod for E_0 – mode.

TBALE A.6.1 : Q as a function of radius of the rod.

$2a/\lambda_0$	Q
0.620	0.089
0.634	0.125
0.651	0.156
0.669	0.186
0.708	0.245
0.746	0.342
0.784	0.357
0.822	0 402
0.ε76	0.474
0.967	0.555
1.153	0.632
1.352	0.654

13. ACKNOWLEDGMENT

The authors are grateful to Dr. S. Dhawan, Director, and also to U.G.C., New Delhi, for permission and encouragement to conduct the project. The authors also expresses their grateful thanks to Dr. James R Wait, Monitor, Senior Scientist *O/T–ITS* for his support, encouragement and technical advice. The U.S. Department of Commerce is also thanked for providing *PL*–480 funds. The authors are also indebted to NOAA for necessary support and encouragement.

14. REFERENCES

1. K. N. Shankara and S. K. Chatterjee — *J. Indian Inst. Sci.*, (Under publication).
2. ——— .. .. *Ibid.*
3. G. A. Deschamps .. .. *J. Appl. Physics*, 1953, **24**, 1046.
4. S. K. Chatterjee and V. Subramanyam — *J. Indian Inst. Sci.*, 1958, **50**, 258.
5. W. M. Elasser .. .. *J. Appl Physics*, 1949, **20**, 1193.

AUTHOR INDEX

Vol. 54 (1972)

TITLE INDEX

Vol. 54 (1972)